Available online at www.sciencedirect.com

ScienceDirect

Geochimica et Cosmochimica Acta 166 (2015) 344–371

Geochimica et Cosmochimica Acta

www.elsevier.com/locate/gca

Beyond temperature: Clumped isotope signatures in dissolved inorganic carbon species and the influence of solution chemistry on carbonate mineral composition

Aradhna K. Tripati [a,b,*], Pamela S. Hill [a], Robert A. Eagle [a,c], Jed L. Mosenfelder [d], Jianwu Tang [a], Edwin A. Schauble [a], John M. Eiler [c], Richard E. Zeebe [e], Joji Uchikawa [e], Tyler B. Coplen [f], Justin B. Ries [g], Drew Henry [a]

[a] *Department of Earth, Planetary, and Space Sciences, University of California, Los Angeles, CA, USA*
[b] *Department of Atmospheric and Oceanic Sciences, Institute of the Environment and Sustainability, California Nanosystems Institute, University of California, Los Angeles, CA, USA*
[c] *Division of Geological and Planetary Sciences, California Institute of Technology, Pasadena, CA, USA*
[d] *Department of Geology and Geophysics, University of Minnesota, Minneapolis, MN, USA*
[e] *Department of Oceanography, SOEST, University of Hawaii, Honolulu, HI, USA*
[f] *U.S. Geological Survey, Reston, VA, USA*
[g] *Department of Marine and Environmental Sciences, Northeastern University, Nahant, MA, USA*

Received 28 July 2014; accepted in revised form 18 June 2015; Available online 7 July 2015

Abstract

"Clumped-isotope" thermometry is an emerging tool to probe the temperature history of surface and subsurface environments based on measurements of the proportion of ^{13}C and ^{18}O isotopes bound to each other within carbonate minerals in $^{13}C^{18}O^{16}O_2^{2-}$ groups (heavy isotope "clumps"). Although most clumped isotope geothermometry implicitly presumes carbonate crystals have attained lattice equilibrium (i.e., thermodynamic equilibrium for a mineral, which is independent of solution chemistry), several factors other than temperature, including dissolved inorganic carbon (DIC) speciation may influence mineral isotopic signatures. Therefore we used a combination of approaches to understand the potential influence of different variables on the clumped isotope (and oxygen isotope) composition of minerals.

We conducted witherite precipitation experiments at a single temperature and at varied pH to empirically determine ^{13}C–^{18}O bond ordering (Δ_{47}) and $\delta^{18}O$ of CO_3^{2-} and HCO_3^- molecules at a 25 °C equilibrium. *Ab initio* cluster models based on density functional theory were used to predict equilibrium ^{13}C–^{18}O bond abundances and $\delta^{18}O$ of different DIC species and minerals as a function of temperature. Experiments and theory indicate Δ_{47} and $\delta^{18}O$ compositions of CO_3^{2-} and HCO_3^- ions are significantly different from each other. Experiments constrain the Δ_{47}–$\delta^{18}O$ slope for a pH effect (0.011 ± 0.001; $12 \geqslant pH \geqslant 7$). Rapidly-growing temperate corals exhibit disequilibrium mineral isotopic signatures with a Δ_{47}–$\delta^{18}O$ slope of 0.011 ± 0.003, consistent with a pH effect.

Our theoretical calculations for carbonate minerals indicate equilibrium lattice calcite values for Δ_{47} and $\delta^{18}O$ are intermediate between HCO_3^- and CO_3^{2-}. We analyzed synthetic calcites grown at temperatures ranging from 0.5 to 50 °C with and without the enzyme carbonic anhydrase present. This enzyme catalyzes oxygen isotopic exchange between DIC species and is present in many natural systems. The two types of experiments yielded statistically indistinguishable results, and these measurements yield a calibration that overlaps with our theoretical predictions for calcite at equilibrium. The slow-growing Devils Hole calcite exhibits Δ_{47} and $\delta^{18}O$ values consistent with lattice equilibrium.

* Corresponding author at: Department of Earth, Planetary, and Space Sciences, 595 Charles Young Drive, University of California, Los Angeles, Los Angeles, CA 90095, USA. Tel.: +1 310 999 5815.
E-mail address: aradhna.tripati@gmail.com (A.K. Tripati).

http://dx.doi.org/10.1016/j.gca.2015.06.021

Factors influencing DIC speciation (pH, salinity) and the timescale for DIC equilibration, as well as reactions at the mineral–solution interface, have the potential to influence clumped-isotope signatures and the $\delta^{18}O$ of carbonate minerals. In fast-growing carbonate minerals, solution chemistry may be an important factor, particularly over extremes of pH and salinity. If a crystal grows too rapidly to reach an internal equilibrium (i.e., achieve the value for the temperature-dependent mineral lattice equilibrium), it may record the clumped-isotope signature of a DIC species (e.g., the temperature-dependent equilibrium of HCO_3^-) or a mixture of DIC species, and hence record a disequilibrium mineral composition. For extremely slow-growing crystals, and for rapidly-grown samples grown at a pH where HCO_3^- dominates the DIC pool at equilibrium, effects of solution chemistry are likely to be relatively small or negligible. In summary, growth environment, solution chemistry, surface equilibria, and precipitation rate may all play a role in dictating whether a crystal achieves equilibrium or disequilibrium clumped-isotope signatures.

1. INTRODUCTION

Clumped isotope thermometry has emerged as a powerful tool in the geosciences (Ghosh et al., 2006; Came et al., 2007; Eagle et al., 2010, 2011,2013a,b; Passey et al., 2010; Csank et al., 2011; Loyd et al., 2012, 2013; Tripati et al., 2010, 2014). The geothermometer exploits systematic changes in the occurrence of multiple rare-isotope substitutions (^{13}C–^{18}O bonds) in carbonate minerals with temperature. To date, only one study has explicitly controlled major factors influencing mineral growth, dissolved inorganic carbon (DIC) speciation and precipitation rate, and explored whether such factors may affect clumped isotope signatures (Tang et al., 2014). A few studies have found evidence for kinetic effects in speleothems (e.g., Affek et al., 2008, 2014; Daëron et al., 2011; Affek and Zaarur, 2014; Kluge et al., 2014) and possibly in other biological systems (e.g., Ghosh et al., 2006; Tripati et al., 2010; Saenger et al., 2012). Ultimately, to assess the limitations of the clumped isotope geothermometer, it is critical to determine the extent to which factors other than temperature affect ^{13}C–^{18}O bond abundance in carbonates.

Our objective in this paper is to provide a comprehensive assessment of the influence of solution chemistry on clumped isotope signatures in DIC species and carbonate minerals. The approaches we use are similar to what have been employed to explore the impact of solution pH on the oxygen isotope composition of the DIC pool and on the widely-used carbonate-water $\delta^{18}O$ geothermometer (e.g., McCrea, 1950; Spero et al., 1997; Zeebe, 1999; Beck et al., 2005; Coplen, 2007; Uchikawa and Zeebe, 2012; Watkins et al., 2013). We present a series of experiments and theoretical calculations exploring the effects of temperature, pH and growth rate on minerals, with results compared to new data for natural samples. We establish the clumped isotope and $\delta^{18}O$ values of aqueous CO_3^{2-} and HCO_3^- and the effects of pH on the DIC pool, by measuring witherite that is quantitatively precipitated from DIC solutions equilibrated at variable pH and a constant temperature. In order to reconstruct the clumped isotope composition of the DIC pool from these data, we report an experimentally-determined acid digestion fractionation factor for witherite. These experimental results are compared to new *ab initio* calculations for the equilibrium isotopic composition of DIC species and carbonate minerals, expanding on our previous theoretical work (Hill et al., 2014). We use these experimental and *ab initio* constraints on endmember CO_3^{2-} and HCO_3^- compositions to determine the compositional dependence of the DIC pool on parameters that influence DIC speciation (i.e., pH, salinity, and temperature). We show that a cultured temperate coral exhibits disequilibrium mineral signatures consistent with a pH effect.

After exploring these kinetic effects, we report observations of possible equilibrium clumped isotope signatures of carbonate minerals, including a new temperature calibration based on synthetic calcites, and the slow-growing Devils Hole calcite vein that is thought to have grown in equilibrium. We also summarize and evaluate published models of equilibrium and disequilibrium isotopic signatures in carbonate minerals, and propose a new interfacial model. Finally we discuss the implications of our results for interpreting data for different types of geological systems, and propose ways to better constrain such effects in the future.

1.1. Background on clumped isotopes

In contrast to $\delta^{18}O$ thermometry, clumped-isotope thermometry does not require knowledge of the isotopic composition of mineral formation waters because it is based on an internal isotope-exchange reaction within the mineral:

$$\text{Reaction 1}: \quad X^{12}C^{18}O^{16}O_2 + X^{13}C^{16}O_3 \leftrightarrow X^{13}C^{18}O^{16}O_2 + X^{12}C^{16}O_3$$

where X refers to cations (e.g., Ca^{2+}, Mg^{2+}). The equilibrium constant (K_{eq}) for this reaction approaches a value of 1 with increasing temperature, resulting in an increasingly random distribution of isotopes among all possible isotopologues in the mineral lattice (Schauble et al., 2006). The quantity Δ_{47} is used to quantify ^{13}C–^{18}O bond ordering in CO_2 derived from acid digestion of minerals, and refers to the deviation in the abundance of CO_2 molecules with a $m/z = 47$ from the abundance predicted by stochastic (random) mixing. Similarly, the Δ_{63} of carbonate ion groups in carbonate-containing compounds (e.g., CO_3^{2-}, HCO_3^-, carbonate minerals) is the deviation in the abundance of the multiply-substituted CO_3^{2-} isotopologue $^{13}C^{18}O^{16}O_2^{2-}$ of m/z 63 from what is predicted by random mixing. These quantities are explicitly defined in Section 2.1.

Most applications of Δ_{47} thermometry implicitly assume that a mineral has attained lattice equilibrium. However, no data exist to constrain what solution equilibrium looks like at a given temperature, pH, and salinity – and how it differs from mineral lattice equilibrium at a given temperature. We also do not know whether mineral disequilibrium may arise from growth from a solution that is in equilibrium. It is also still unclear which of several Δ_{47}–temperature calibrations reflects mineral equilibrium: various experimental Δ_{47}–temperature calibrations have been derived using different synthesis methods from carbonates grown under controlled temperatures that exhibit different slopes and intercepts (e.g., Ghosh et al., 2006 and Zaarur et al., 2013 vs. Dennis and Schrag, 2010 and Tang et al., 2014). An additional complicating factor is that discrepancies may at least in part arise from analytical artifacts (acid digestion temperature, acid density, CO_2 extraction and purification system used) and not just differences in synthesis (Dennis et al., 2011; Defliese et al., 2015), as has been shown to be important for oxygen isotope measurements (Swart et al., 1991).

Many natural samples of modern carbonates with independent constraints on growth temperature yield Δ_{47} values cluster within 0.02‰ around synthetic calibrations obtained using the same analytical approach, and are therefore presumed to be statistically indistinguishable from mineral equilibrium (Ghosh et al., 2006; Eagle et al., 2010; Eiler, 2011; Thiagarajan et al., 2011). Even so, deviations from these calibrations of up to −0.10‰ have been reported in speleothems (e.g., Affek et al., 2008; Daëron et al., 2011; Kluge and Affek, 2012). Disequilibrium mineral signatures have also been reported for tropical corals, and possibly observed in benthic foraminifera from near-freezing water temperatures (Ghosh et al., 2006; Affek et al., 2008; Tripati et al., 2010; Daëron et al., 2011; Saenger et al., 2012).

An explanation for some of the reported variation in calibration datasets is that some carbonate minerals are not attaining thermodynamic isotopic equilibrium within the mineral lattice itself (referred to as lattice equilibrium, or the thermodynamic equilibrium for a mineral, as opposed to thermodynamic equilibrium for a solution). Instead, mineral isotopic signatures may be impacted by multiple kinetic and thermodynamic factors near the site of crystal growth, with solution and crystal growth kinetics playing a role in governing mineral clumped isotope signatures (Eagle et al., 2010; Tripati et al., 2010; Kluge et al., 2014; Tang et al., 2014). If this hypothesis is correct, minerals may record an isotopic fingerprint of processes in the solution and at the mineral–solution interface. If different DIC species have different clumped isotope signatures (as with $\delta^{18}O$), then for crystals growing from a DIC pool at equilibrium, the Δ_{63} of minerals may therefore be affected by factors influencing the proportions of CO_3^{2-} and HCO_3^- in solution (such as pH, salinity, and temperature) as well as growth rate. Thus, clumped isotope signatures of carbonate minerals could differ from the theoretical mineral equilibrium for many combinations of pH, salinity, temperature, and growth rate. Similarly, if clumped-isotope signatures in DIC species differ from their equilibrium state (for example, due to kinetic isotope effects associated with transport or chemical reactions), then disequilibrium Δ_{63} values might be recorded by carbonate minerals. Thus, solution chemistry may explain, in part, the scatter in Δ_{47} values observed for carbonate minerals formed at the same temperature.

2. MATERIALS AND METHODS

2.1. Definitions of Δ_n, α^n, and β^n values

^{13}C–^{18}O bond order in CO_2 is described using the quantity Δ_{47}, which refers to the deviation in the abundance of CO_2 molecules with a $m/z = 47$ from the abundance predicted by stochastic (random) mixing. Specifically, the quantity Δ_{47} is defined as:

$$\Delta_{47} = \frac{R^{47}}{2R^{13}R^{18} + 2R^{17}R^{18} + R^{13}(R^{17})^2} - \frac{R^{46}}{2R^{18} + 2R^{13}R^{17} + R^{13}(R^{17})^2} - \frac{R^{45}}{R^{13} + 2R^{17}} + 1$$

where R is the number ratio (Coplen, 2011), the number of a minor isotopologue to the number of the major isotopologue of a specified molecule (or atom) of interest. Similarly, the Δ_{63} of carbonate ion groups in carbonate-containing compounds (including, but not limited to CO_3^{2-} ions, HCO_3^- ions, and carbonate minerals such as calcite and witherite) is the deviation in the abundance of the multiply-substituted CO_3^{2-} isotopologue $^{13}C^{18}O^{16}O_2$ of m/z 63 from the abundance predicted by random mixing.

The quantities Δ_{48}, Δ_{49}, Δ_{64}, Δ_{65}, Δ_{66}, and Δ_{67} are defined in a similar manner. Because the Δ_{63} of carbonate-containing compounds cannot yet be measured directly, the carbonate must first be converted to CO_2 by phosphoric acid digestion and then measured in a gas-source isotope ratio mass spectrometer (Ghosh et al., 2006). The Δ_{47} of a sample is related to the Δ_{63} of the same sample by correcting for isotopic fractionation that occurs during acid digestion, such that:

$$\Delta_{47} = \Delta_{63} + y$$

where y is the fractionation factor for a given acid digestion temperature. The quantity y is also predicted to have a slight dependence on mineral isotopic composition and state of ordering (Guo et al., 2009). Experimental and theoretical constraints on acid digestion fractionation factors for converting Δ_{63} to Δ_{47} for different carbonate minerals are discussed below.

The isotopic fractionation factor α_{A-B} is used to describe the isotopic fractionation between 2 phases A and B (e.g., two DIC species, or $CaCO_3$ and H_2O) such that:

$$\alpha^{18O}_{A-B} = R(^{18}O/^{16}O)_A / R(^{18}O/^{16}O)_B$$

The symbol β^{18O} is defined as the $^{18}O/^{16}O$ partitioning between a given species and gas phase oxygen atoms:

$$\beta^{18O}_{CO_3^{2-}} = \alpha^{18O}_{CO_3^{2-}} - O_{(g)}$$

It follows that $\alpha^{18O}_{A-B} = \beta^{18O}_A / \beta^{18O}_B$.

2.2. Experimental methods

2.2.1. Quantitative DIC precipitation experiments

As the clumped isotope composition of DIC cannot be measured *in situ*, we used the standard method of witherite precipitation as a tool for determining solution composition. After equilibrating a solution of DIC, the addition of $BaCl_2$ results in the quasi-instantaneous and complete transformation of the total DIC pool into solid witherite. The resultant $BaCO_3$ records the $\delta^{18}O$ and the $\delta^{13}C$ values of the total DIC pool at the time of mineral precipitation. Hence, this technique has been applied as a tool to constrain the respective isotopic compositions of the DIC species and to characterize isotopic fractionation in the CO_2–H_2O system (McCrea, 1950; Usdowski et al., 1991; Beck et al., 2005; Uchikawa and Zeebe, 2012, 2013). Such isotopic fractionations in solution can potentially be reflected in both synthetic and natural carbonate minerals. This process has in turn been used to explain some of the classic observations of disequilibrium mineral oxygen isotope signatures in natural samples of calcite and aragonite, such as in foraminifera and deep-sea corals (Spero et al., 1997; Adkins et al., 2003).

To characterize Δ_{47} signatures of HCO_3^- and CO_3^{2-} that are in complete isotopic equilibrium with H_2O, we analyzed a subset of witherite ($BaCO_3$) samples from Uchikawa and Zeebe (2013). Witherite was quantitatively precipitated under controlled conditions at 25 °C (Table S1) from parent solutions of sodium bicarbonate in adherence to a published protocol (Beck et al., 2005); details of the experiments are described elsewhere (Uchikawa and Zeebe, 2012, 2013).

In total, 17 samples were precipitated at pH values between 7.8 and 12.0 in order to span a wide range of solution HCO_3^-/CO_3^{2-} ratios (Fig. 1; Tables S1 and S2). At a given temperature, the timescale for achieving isotopic equilibrium is pH dependent (e.g., Beck et al., 2005). Therefore, solutions were equilibrated for time intervals substantially longer than the timescale required for oxygen isotopic equilibration at respective pH values (Usdowski et al., 1991; Zeebe and Wolf-Gladrow, 2001; Beck et al., 2005; Uchikawa and Zeebe, 2013), which is thought to be similar to the timescale for achieving clumped-isotope equilibrium (Affek, 2013). The DIC pool in the parent solution was then precipitated quantitatively and near-instantaneously using established methods (Beck et al., 2005; Uchikawa and Zeebe, 2013). Thus the $\delta^{18}O$ values of these samples should reflect those of the DIC pool in the parent solutions (McCrea, 1950; Usdowski et al., 1991; Beck et al., 2005).

The pH of parent solutions was measured with two Orion pH electrodes calibrated daily with three Orion pH buffers that are referenced to NIST standards. Parent $NaHCO_3$ solutions were prepared using CO_2-free water to achieve a DIC concentration of 15 mM. Therefore all the DIC in the solution was only contributed from $NaHCO_3$ powder (which is homogeneous in terms of $\delta^{13}C$ and $\delta^{18}O$). The pH of $NaHCO_3$ solutions was modified to a specified value by adding either HCl or NaOH solutions, which were also prepared with CO_2-free water. At pH 7.8, HCO_3^- is ~2 orders of magnitude more abundant than CO_3^{2-} (Fig. 1), and at pH 10.2 HCO_3^- and CO_3^{2-} are present at similar concentrations. At pH 12.0, CO_3^{2-} comprises ~98% of the DIC pool.

$NaHCO_3$ solutions were equilibrated in a thermostat-controlled water bath (25 ± 0.04 °C) at specified pH values. The equilibrated $NaHCO_3$ solution was then transferred to a N_2-filled bottle containing excess $BaCl_2$ powder, and concentrated NaOH solution was immediately added to the mixture to trigger $BaCO_3$ precipitation. Based on stoichiometric calculations for these experiments (Uchikawa and Zeebe, 2013), nearly all of the DIC in the $NaHCO_3$ solution was trapped quasi-instantaneously as $BaCO_3$. The $\delta^{13}C$ of the witherite samples also was compared to the only carbon source for the experiments (i.e., the $NaHCO_3$, which had a $\delta^{13}C$ of $-2.89 \pm 0.02‰$). The agreement between the $\delta^{13}C$ values for the witherite and $NaHCO_3$ indicates that the samples analyzed were quantitatively precipitated and not influenced by partial removal of DIC and/or contaminated by atmospheric CO_2 or dissolved CO_2 in the water used for precipitation (Uchikawa and Zeebe, 2013). Using pH, DIC, and $\delta^{18}O$ values of the water provided by Uchikawa, the speciation of DIC was calculated using the experimental curves for K_1 and K_2 (Millero et al., 2006) using the program CO_2sys (Lewis et al., 1998; Pierrot et al., 2006).

Thus, the Δ_{47} and $\delta^{18}O$ of resultant $BaCO_3$ reflects the ^{13}C–^{18}O bond abundance and the $\delta^{18}O$ of the sum of the DIC species in the $NaHCO_3$ solution at the time of mineral precipitation. Samples were analyzed using X-ray diffraction to ensure that witherite was the only mineral present. A more detailed discussion of these precipitation experiments is provided in Uchikawa and Zeebe, 2013.

2.2.2. Heating experiments and mineral-specific acid digestion fractionation factors

Mineral heating experiments were performed at high pressure and temperature using an end-loaded piston-cylinder apparatus in order to randomize isotopic distributions within samples. Following the procedures used in Ghosh et al. (2006) and Guo et al. (2009), carbonate minerals were heated to a temperature above their melting point (monitored with a thermocouple), and then quenched to produce a stochastic distribution. For our experiments, the starting material was natural witherite from Settlingstones Mine (Fourstones, Northumberland, England), which was mixed with reagent-grade $BaCl_2$ in 1:1 M proportions and loaded into 4-mm (diameter) platinum capsules. $BaCl_2$ was added in order to achieve eutectic melting at a temperature below the high-pressure melting curve of $BaCO_3$, following 1-atm data from Chandra (1981). The capsules were welded, inserted into 12.7-mm $BaCO_3$–graphite cell assemblies and subjected to nominal conditions of 1650 °C and 3 GPa for durations of 15–22 h. The experiments were conducted using hot piston-in technique with a nominal pressure correction of −0.2 GPa, with calibration details described in Xirouchakis et al. (2001). Temperature was monitored and controlled using type B thermocouples (Pt70–Rh30–Pt94–Rh6), uncorrected for the effect of pressure on

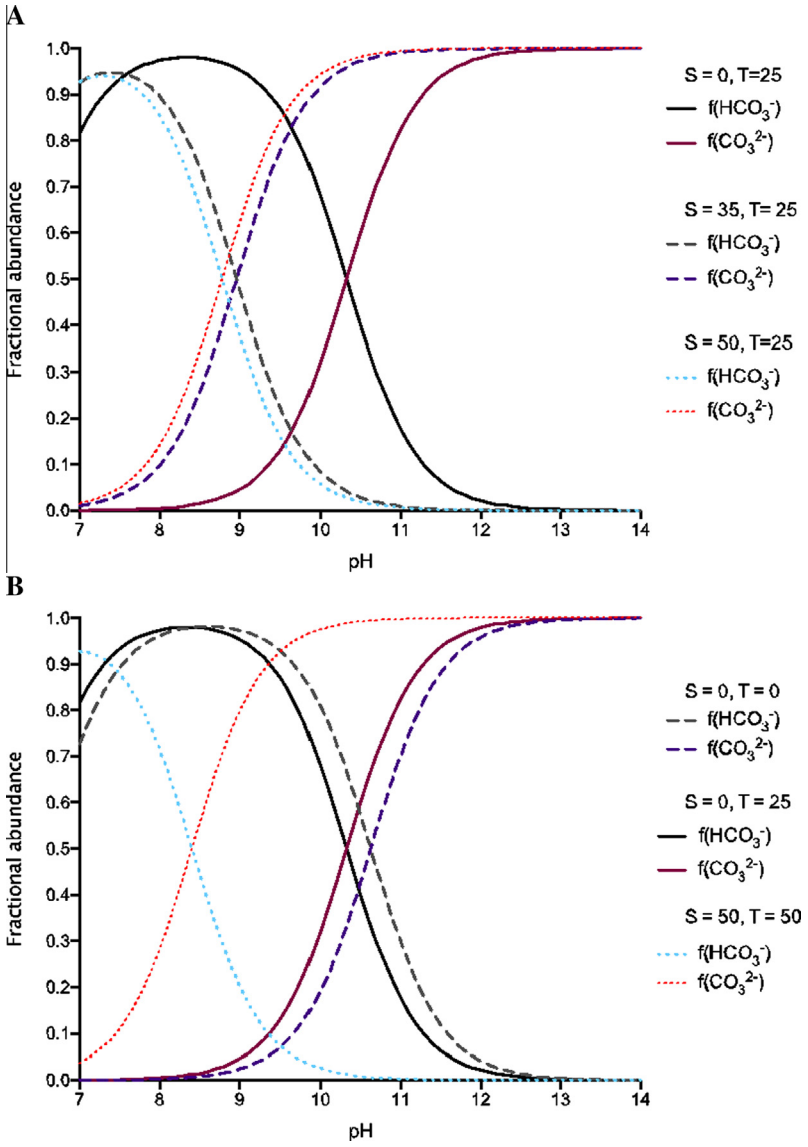

Fig. 1. Bjerrum plot showing calculated fractional abundance of bicarbonate and carbonate ions as a function of pH, salinity, and temperature. (A) DIC speciation as a function of pH and salinity at 25 °C. This panel shows the influence of changing salinity on DIC speciation. (B) DIC species abundance as a function of pH, salinity, and temperature. This panel demonstrates both the effects of only changing temperature, and the combined effects of temperature and salinity, on DIC speciation.

electromotive force. Experimental charges were quenched rapidly by turning off power to the furnace, resulting in cooling to below 200 °C in 20 s and to room temperature within 1 min. Crystalline-run products were recovered by stripping off the Pt capsule. X-ray diffraction was used to verify the presence of $BaCO_3$ and $BaCl_2$.

Samples with a stochastic distribution of isotopologues were then digested in phosphoric acid and analyzed to quantify the mineral-specific acid digestion fractionation factor (AFF), assuming the materials had a composition of 0‰. Calculated mineral-specific AFF to convert Δ_{63} to Δ_{47} are shown in Table 1. Theoretical AFF for calcite from Guo et al. (2009) were used to convert Δ_{64} and Δ_{65} to Δ_{48} and Δ_{49} on the stochastic reference frame.

2.2.3. Synthetic calcite precipitation experiments

Synthetic calcite was grown at a range of temperatures using a published methodology used previously for calibrating the relationship between $\delta^{18}O$ and temperature (Kim and O'Neil, 1997), and Δ_{47} and temperature (Ghosh et al., 2006; Zaarur et al., 2013). CO_2 was bubbled for about an hour through a stirred 1-L solution containing $CaCO_3$ powder (Carrara Marble calcite, Mallinckrodt calcite, Sigma–Aldrich calcite, and coral aragonite were used). To remove undissolved particles, the solution was filtered through an 8 μ filter.

Two hundred fifty milliliters of solution was then transferred to an Erlenmeyer flask and placed in a temperature-controlled water bath. Water temperatures

Table 1
Acid digestion fractionation factors from experimental data (reaction temperature of 25 °C) for converting Δ_{63} to Δ_{47}. ARF = absolute reference frame; s.e. = standard error; s.d. = standard deviation. Bold values represent mineral-specific average.

Mineral	Δ_{47} (‰, ARF)	1 s.e.	Source
Calcite	**0.280**	0.016 (1 s.d.)	
Calcite – MZ carb	0.283	0.014	Recalculated in this study using data from Guo et al. (2009)
Calcite – sigma carb	0.292	0.009	Recalculated in this study using data from Guo et al. (2009)
	0.288	0.009	Recalculated in this study using data from Guo et al. (2009)
Calcite – NBS-19	0.256	0.012	Recalculated in this study using data from Guo et al. (2009)
Witherite	**0.255**	0.006 (1 s.d.)	
Witherite – B644	0.259	0.007	Experimentally determined in this study.
Witherite – A1240	0.251	0.008	Experimentally determined in this study.

for some experiments were 0.5 ± 0.5 °C and were maintained using an ice–water mixture in the bath. Other experiments were conducted at 25, 27, 30, 40, and 50 °C (±1 °C) (Table S3) and solutions equilibrated for three days with temperatures maintained in a heated water bath. For the lowest temperature experiments, solutions were allowed to equilibrate for up to a week.

Some experiments were conducted under identical conditions but with 0.2 mg/mL of bovine carbonic anhydrase (Sigma–Aldrich) added to the solution. The enzyme catalyzes isotopic equilibrium in the hydrolysis of CO_2 and achieves rapid oxygen isotopic equilibration among DIC species (Uchikawa and Zeebe, 2012; Watkins et al., 2013). While the enzyme may not be active at 50 °C, we can expect activity at all of the other temperatures studied. The pH was monitored twice a day as an assay to verify activity (Uchikawa and Zeebe, 2012), and precipitation was induced after the solution pH had stabilized.

Precipitation of calcite was forced by slowly bubbling N_2 gas through the solution using a partially submerged Pasteur pipette inserted through a rubber stopper in the flask. The flow rate was monitored using a flow meter and maintained at 10 mL/min. The bubbling of N_2 gas through the solution displaced CO_2, thereby elevating the pH and saturation state of the solution to the point of calcite precipitation.

After 1–5 days, the experiment was terminated and the precipitate was filtered. Precipitate was also scraped off the sides and bottom of the flask using a spatula. Samples were air-dried for two days and stored in sealed glass vials in a desiccator until analysis. Mineralogy was checked using X-ray diffraction. Only samples containing pure calcite were analyzed. Both aragonite and vaterite were occasionally observed in some X-ray diffraction patterns, and these samples were discarded.

2.2.4. Temperate coral culture experiments

We measured cultured specimens of the temperate coral *Oculina arbuscala* (Table S4) that were grown as part of a published study and detailed methods are in this publication (Ries et al., 2009). Briefly, field-collected specimens of the zooxanthellate temperate coral *Oculina arbuscula* were cultured for 60 days at pH values of 8.11 ± 0.06 (1σ), 7.85 ± 0.05, and 7.48 ± 0.03 manipulated by bubbling CO_2 (Ries et al., 2009, 2010; Table S4). Temperature was maintained at 25.0 ± 0.1 °C (1σ), salinity at 31.6 ± 0.4 (1σ), and total alkalinity at 2020 ± 36 μM (1σ). Average rates of calcification for the corals are reported in Table S4. After completion of the experiment, skeletal aragonite formed exclusively under the experimental conditions (identified relative to a $^{137}Ba/^{138}Ba$ spike emplaced at the start of the experiment) was extracted from the corals by scalpel under a stereomicroscope and analyzed for Δ_{47} and $\delta^{18}O$.

2.2.5. Stable isotope analyses

Approximately 7–12 mg of $BaCO_3$ or 5–8 mg of $CaCO_3$ samples were reacted for 20 min with phosphoric acid ($\rho = 1.92$ g/mL) on a 90 °C online common acid bath system described in detail elsewhere (Passey et al., 2010), with acid typically changed every 10–15 analyses. Briefly, CO_2 gas was immediately passed through a dry ice/ethanol trap to remove water and frozen with liquid nitrogen. Cryogenic purification of CO_2 was achieved using an automated online vacuum line. Additional automated sample cleanup steps included passing sample gas through a Porapak Q™ 120/80 mesh GC column at −20 °C to remove potential organic contaminants and silver wool (Sigma–Aldrich) to remove sulfur compounds. The $\delta^{13}C$, $\delta^{18}O$, Δ_{47} and Δ_{48} of CO_2 evolved from the phosphoric acid digestion of carbonates were determined on three Thermo Scientific MAT 253 gas-source mass spectrometers based at Caltech and UCLA that are configured identically, using published methods (Ghosh et al., 2006; Huntington et al., 2009; Eagle et al., 2010, 2011; Passey et al., 2010; Tripati et al., 2010). Samples were analyzed ensuring that m/z-44 voltages remained stable at 16 V throughout the course of each analysis. With the exception of the heating experiment products, all sample types (witherite precipitation experiments, Devils Hole vein carbonates, calcite precipitation experiments, and coral samples) were run on all three instruments. Heating experiment products were run exclusively at UCLA. Carbonate standards were analyzed between every 3–5 samples and were prepared and analyzed in the same manner as samples.

In order to confirm the purity of cleaned CO_2 samples, we screened for the presence of contaminating molecules such as hydrocarbons and sulfur compounds using m/z-48 anomalies. Sample Δ_{48} values are referenced to a stochastic distribution. Large deviations of over 1‰ are considered potentially indicative of the presence of contaminants,

and these measurements are excluded from further analysis. In total, we conducted 155 analyses including replicates (excluding standards) that were comprised of 17 samples from the witherite precipitation experiments, 12 samples from the calcite precipitation experiments, two samples from the heating experiments, six samples from the Devils Hole calcite vein, and nine temperate coral samples. Data for 10 analyses (including for one entire sample from the DIC precipitation experiments) were excluded due to Δ_{48} excesses or $\delta^{13}C$ or $\delta^{18}O$ values that deviated from the population mean by more than 3σ, which are interpreted to reflect incomplete acid digestion or equilibration with water, and/or contamination.

2.2.6. Calculations to derive stable isotope values and their errors

Data for heating experiments to determine AFF, witherite precipitation experiments, synthetic calcite, coral aragonite, and the Devils Hole calcite vein are reported in Tables 1, and S2–S5 respectively. A comparison of Δ_{47} values for 25 and 33.7 °C constrained using data from this study to predictions from several experimental and empirical calibrations, and to our theoretical results, is shown in Table 2. 25 °C was selected because it corresponds to the temperature of our quantitative DIC precipitation experiments and cultured temperate coral experiments, and 33.7 °C is shown because it is present-day temperature of growth for the Devils Hole system.

For all samples, equilibrated gases were used for a non-linearity correction. All Δ_{47} values are reported on the absolute reference frame (ARF), calculated using gases equilibrated at 25 and 1000 °C, following a standard procedure (Dennis et al., 2011) and with the acid digestion correction of Henkes et al. (2013) of 0.092‰ added after projection onto ARF, which is similar to the value reported by Defliese et al. (2015).

We also recalculate AFF for calcite using published experimental data from Guo et al. (2009). These data were reported relative to the stochastic distribution. For this study, reported Δ_{47} values are projected onto ARF using a secondary transfer function based on heated gases and their reported standard values for NBS 19 (0.334‰ relative to the stochastic distribution). A secondary transfer function was calculated using NBS 19 values of 0.392‰ and a 1000 °C-equilibrated CO_2 value of 0.0266 derived from Dennis et al. (2011), with a slope of 1.09401 and intercept of 0.0266.

We ran an in-house Carrara Marble standard (which was analyzed the most frequently), a NBS 19 standard, and a vein calcite in-house standard (102-GC-AZ01) and note that standard values on the stochastic reference frame are comparable between instruments at Caltech and UCLA. The average measured value for Carrara Marble for Caltech Mass Spectrometer 1 is 0.394 ± 0.006‰ ($n = 12$), and on Caltech Mass Spectrometer 2 is 0.395 ± 0.004‰ ($n = 10$). The average measured value on the instrument at UCLA is 0.386 ± 0.002‰ ($n = 72$). Uncertainties in reported Δ_{47} values and calculated temperatures include the propagated uncertainty in equilibrated gas determination and in sample measurements. NBS-19 ($\delta^{13}C_{V\text{-}PDB} = -2.2$‰ and $\delta^{18}O_{V\text{-}PDB} = 1.95$‰) was used to normalize carbonate $\delta^{18}O$ and $\delta^{13}C$ data, which are reported relative to the V-PDB standard. The $\delta^{18}O$ of water is from Uchikawa and Zeebe, 2013 and is reported relative to the V-SMOW standard.

For calcite, $^{18}O/^{16}O$ fractionation by phosphoric acid digestion at 90 °C was corrected using a fractionation factor of 1.007954 (Swart et al., 1991). For aragonite, a value of 1.00854126 was calculated by extrapolating the relationship reported by Kim et al. (2007) to a reaction temperature of 90 °C. For witherite, an acid digestion oxygen isotopic fractionation factor of 1.009276 was used for $\delta^{18}O$ calculations, based on the recalculated value from Guo et al. (2009) using data originally reported by Böttcher (1996). It should be noted that other studies have chosen to use a different acid digestion fractionation factor to calculate $\delta^{18}O$ values of witherite. The study of Beck et al. (2005) argued that the calcite–witherite difference is small and used a published calcite oxygen isotopic fractionation factor from another study (Kim and O'Neil, 1997); the Uchikawa and Zeebe (2013) study used a calcite fractionation factor because the witherite fractionation factor, although conceptually proper, is not well-constrained. Calculated $\delta^{18}O$ and $1000\ln\alpha^{18O}$ values for each sample, using both oxygen isotopic fractionation factors for completeness, are presented in Table S2. All figures and data tables show calculations using both fractionation factors for the sake of completeness; however, it should be noted that the choice of value does not compromise the trends in our results or affect our conclusions.

2.2.7. Determining end-member DIC species stable isotopic compositions

Using an isotopic mass balance, HCO_3^- and CO_3^{2-} end-member stable isotopic compositions (Table 2) were calculated from each sample that was from a solution with >90% of either species. Reported end-member HCO_3^- and CO_3^{2-} estimates were then derived from the three highest (CO_3^{2-} fraction of ~90% or greater) and four lowest (HCO_3^- fraction of 96% or greater) pH experiments.

2.3. Model calculations for equilibrium stable isotopic compositions of DIC species

In this study, we focused on modeling the isotopic composition of DIC species and carbonate minerals on the same computational framework (Tables 2, 3, and S6–S7). In an in-depth study of solvation modeling techniques coupled with different levels of theory that is described in a companion paper (Hill et al., 2014), we determined an optimal model that was both computationally efficient and reasonably accurate. Here, we used the data from Hill et al. (2014) and conducted additional modeling experiments. We use a supermolecular cluster model (species surrounded by 21–32 water molecules) using the *ab initio* density functional theory (DFT) method B3LYP in combination with the 6-311++G(2d,2p) Pople basis set. For witherite calculations, we used the B3LYP model with the SDD basis set. This basis set was selected because the 6-311++G(2d,2p) basis set does not include Ba.

Table 2
Summary of stable isotope predictions of Δ_{47} for 25 °C and 33.7 °C based on analytical and theoretical components of this study. AFF refers to acid digestion fractionation factor. Errors in the determination of the acid digestion fractionation factor are not folded into these estimates as they are poorly constrained and perhaps best represented by the range of values determined using the two different mineral-specific AFF.

Data	Temperature (°C)	Witherite-specific AFF		Calcite AFF	
		Δ_{47} (‰, ARF)	1 s.e.	Δ_{47} (‰, ARF)	1 s.e.
Estimates derived using new data from this study					
HCO_3^-	25	0.688	0.001	0.713	0.001
CO_3^{2-}	25	0.625	0.006	0.650	0.006
Predicted from empirical calibrations					
Calcite – this study	25			0.687	
Mixed – Eagle et al. (2013a) all biogenics refit	25			0.700	
Calcite – Dennis and Schrag (2010) refit	25			0.698	
Calcite – Ghosh et al. (2006) refit	25			0.700	
Mixed – Zaarur et al. (2013) refit	25			0.703	
		Witherite-specific AFF Δ_{47} (‰, ARF)		Calcite AFF Δ_{47} (‰, ARF)	
Predictions from theory (cluster model from this study)					
HCO_3^-	25	0.658		0.683	
CO_3^{2-}	25	0.625		0.650	
Calcite	25			0.674	
Aragonite	25			0.686	
Estimate derived using new data from this study					
Devils Hole (this study)	33.7			0.655	0.004
Predicted from empirical calibrations					
Calcite – this study	33.7			0.655	
Mixed – Eagle et al. (2013a) all biogenics refit	33.7			0.664	
Calcite – Dennis and Schrag (2010) refit	33.7			0.677	
Calcite – Ghosh et al. (2006) refit	33.7			0.661	
Mixed – Zaarur et al. (2013) refit	33.7			0.664	
				Calcite AFF Δ_{47} (‰, ARF)	
Predictions from theory (cluster model from this study)					
Calcite	33.7			0.651	

We used the speciation equations from Millero et al. (2006) to compute more detailed tables of salinity and temperature effects on Δ_{63}, β^{13C}, and β^{18O} for comparison with our experimental results. These species abundances were used to estimate the Δ_{63} of total solution DIC. Theoretical Δ_{63} values for the DIC pool were converted to predictions for measured Δ_{47} values using an AFF so that we can compare theoretical calculations to experimental data.

3. RESULTS

Our results indicate that DIC speciation influences the clumped and oxygen isotopic composition of the composite DIC pool, and that solution chemistry may affect the composition of rapidly-grown minerals. Below we estimate the possible effects of DIC speciation on clumped isotope signatures of the DIC pool and carbonate minerals. First we report acid digestion factors for calcite and witherite that are necessary for the interpretation of some of our experimental results. Then we present experimental constraints on the relationship between pH and the Δ_{47} of the DIC pool from witherite precipitation experiments, estimate the equilibrium composition of HCO_3^- and CO_3^{2-}, and experimentally determine a Δ_{47}–$\delta^{18}O$ slope for a "pH effect". Results from experiments are then compared with theoretical predictions. Next we look at DIC speciation effects on carbonate minerals, grown under either equilibrium or disequilbrium conditions. We present data for cultured temperate coral, synthetic calcites grown at variable temperature, and natural samples from the Devils Hole vein.

3.1. Equilibrium isotope effects in solutions

3.1.1. Mineral-specific acid digestion fractionation factors

Precipitation experiments involved precipitating DIC equilibrated at variable pH as witherite. To facilitate comparison of Δ_{47} results for witherite to calcite or aragonite, we experimentally determined mineral-specific AFF. The AFF of witherite and calcite were determined to be 0.255 ± 0.006‰ (1σ) and 0.280 ± 0.016‰ (1σ), respectively (Table 1). The difference in AFF between witherite and calcite (0.025 ± 0.017‰) is similar in magnitude and direction

Table 3
Summary of slopes and intercepts through theoretical predictions of the relationship between bond order and $10^6/T^2$ (T in K). Values were calculated every 5° between 0 and 100 °C and use our determined AFF for calcite, or a mineral-specific AFF (Table 2). To calculate Δ_{63}, subtract 0.280 from the intercept; to calculate Δ_{64}, subtract 0.137; to calculate Δ_{65}, subtract 0.592.

Species	Model	Δ_{47} (ARF): no mineral-specific AFF		Δ_{47}: mineral specific fractionation factor	Δ_{48}: stochastic distribution		Δ_{49}: stochastic distribution	
		Slope	Intercept	Intercept	Slope	Intercept	Slope	Intercept
HCO_3^-	Cluster model (B3LYP/6–311++G(2d,2p))	0.03840	0.2504	Subtract 0.025	0.01439	0.08133	0.09379	0.4793
CO_3^{2-}	Cluster model (B3LYP/6–311++G(2d,2p))	0.03636	0.2403	subtract 0.025	0.01568	0.07884	0.09094	0.4538
Calcite	Cluster model (B3LYP/6–311++G(2d,2p))	0.03753	0.2508	Same	0.01586	0.07887	0.09353	0.4755
Calcite	Cluster model (B3LYP/6 (SDD))	0.03510	0.2511	Same	0.01304	0.08665	0.08577	0.4837
Calcite	Lattice model	0.03938	0.2395	Same				
aragonite	Cluster model (B3LYP/6–311++G(2d,2p))	0.03811	0.2558	subtract 0.002	0.01583	0.07824	0.09508	0.4827
Aragonite	Cluster model (B3LYP/6 (SDD))	0.03533	0.2534	Subtract 0.002	0.01306	0.08549	0.08637	0.4861
Aragonite	Lattice model	0.03358	0.2421	Subtract 0.002				
Witherite	Cluster model (B3LYP/6 (SDD))	0.03476	0.2436	Subtract 0.025	0.03476	0.1006	0.01274	0.5411
Dolomite	Lattice model	0.03873	0.2425	Subtract 0.017				
Magnesite	Lattice model	0.03331	0.253	Subtract 0.033				

to predictions based on transition state theory (0.015‰) (Guo et al., 2009). Furthermore, the observed AFF of 0.280‰ for calcite reconciles observations of high-temperature calcite mineral equilibrium (Passey and Henkes, 2012) with theoretical predictions (Schauble et al., 2006; Hill et al., 2014; this study).

To convert Δ_{63} values for the DIC pool to predictions for measured Δ_{47} values, we calculated clumped-isotope values using two alternate assumptions about AFF that are consistent with these results: (1) the average measured difference between calcite and witherite AFF is 0.025‰, or (2) the AFF for witherite is identical to calcite (0.280‰), given the overlapping 2σ error bars. In light of the errors, we cannot rigorously distinguish between these possibilities. Both acid digestion fractionation factors are included for completeness since there is not yet a consensus within the research community about which acid fractionation factor(s) to use. However, the choice of fractionation factor does not affect the conclusions of this study because the experimental results focus on differences between HCO_3^- and CO_3^{2-} and involve comparisons of data derived only from digestion of witherite. The uncertainty in AFF does affect comparisons between absolute clumped isotope compositions of carbonate minerals and the equilibrium DIC species values inferred from the witherite precipitation experiments, and therefore such comparisons should be made with caution.

3.1.2. Experimental constraints on DIC endmember compositions from witherite precipitation

To investigate whether a discernible difference exists in ^{13}C–^{18}O bond abundance in aqueous HCO_3^- and CO_3^{2-},witherite precipitated from solutions equilibrated at 25 °C and fixed pH values ranging from 7.8 to 12.0 was measured. The Δ_{47} values range from 0.64‰ to 0.72‰ when the calcite AFF is used, and samples grown from HCO_3^--dominated solutions have higher Δ_{47} values than samples grown from CO_3^{2-}-dominated solutions (Fig. 2**A**). We identified a pH dependence of Δ_{47} (Fig. 2A; Table S2); the observed relationship shown in Fig. 2**A** mirrors the effect of pH on HCO_3^- abundance, as well as on bulk mineral $\delta^{18}O$ (Fig. 2B).

As pH increases, the $\delta^{18}O$ of the total DIC pool decreases, and the decrease is recorded in witherite. Samples precipitated at a pH of 7.80–8.90, where HCO_3^- is over 95% of DIC, indicate an oxygen isotopic fractionation between HCO_3^- and water ($1000\ln\alpha^{18O}_{HCO3–H2O}$) of 29.41 ± 0.08 (using a witherite-specific AFF). The highest pH experiments yield $1000\ln\alpha^{18O}$ for CO_3^{2-} of 23.70 ± 0.11 ($1000\ln\alpha^{18O}_{CO3–H2O}$). Calculations with a calcite AFF yield slightly larger $1000\ln\alpha^{18O}_{HCO3–H2O}$ of 30.87 ± 0.11, and 24.79 ± 0.11 for $1000\ln\alpha^{18O}_{CO3–H2O}$, in agreement with previous work (Uchikawa and Zeebe, 2013). The $\delta^{13}C$ of witherite matches the $\delta^{13}C$ of the parent $NaHCO_3$ and neither Δ_{47} nor $\delta^{18}O$ values are significantly correlated with $\delta^{13}C$, as expected for quantitative precipitations of DIC.

Results for these samples (Fig. 2A, Table 2) constrain the Δ_{47} value for HCO_3^- as 0.688 ± 0.001‰ (1 s.e.) and CO_3^{2-} as 0.625 ± 0.006‰, when a witherite-specific AFF is used. With a calcite-specific AFF, values increase to

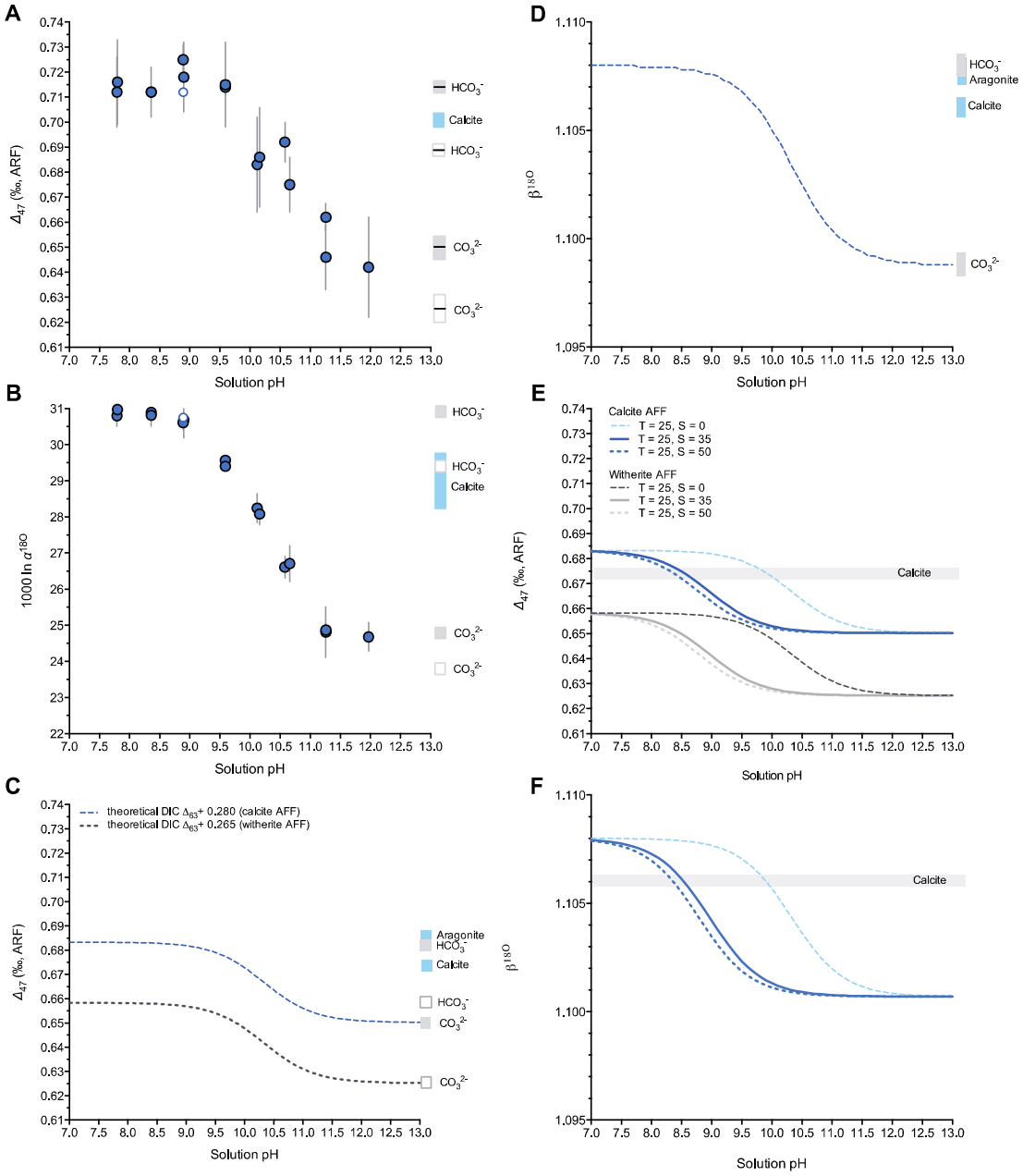

Fig. 2. Experimental and theoretical constraints on Δ_{47} and $\delta^{18}O$ of DIC pool as a function of pH and salinity for solutions equilibrated at 25 °C. (A) Measured Δ_{47} values of total DIC produced from solutions equilibrated at variable pH. For comparison, predictions of mineral Δ_{47} is shown from previous work on synthetic calcite (Ghosh et al., 2006; Dennis and Schrag, 2010; Zaarur et al., 2013) as a blue shaded rectangle, with thickness representing range of values from different calibrations. Also shown are estimated Δ_{47} values for HCO_3^- end-member ($0.713 \pm 0.001‰$; 1 s.e.) and CO_3^{2-} end-member ($0.650 \pm 0.006‰$) from this study (grey symbols, right-hand side) assuming no difference in the acid digestion fractionation factor (AFF) between calcite and witherite. The thin line represents end-member estimates, and bar thickness represents 1 s.e. uncertainty. Note that all values from precipitation experiments including estimates of HCO_3^- and CO_3^{2-} end-members are reduced if a witherite-specific AFF (as determined by the heating experiments) is used (open bars). Application of this fractionation factor would shift HCO_3^- values so they are closer to calcite values. The difference between the gray and open bars reflects a possible AFF difference between witherite and calcite. Open circle represents sample with anomalous $\delta^{13}C$ value (inclusion or exclusion of this sample does not change findings). Average external reproducibility of samples and standards is 0.009‰. (B) The measured oxygen isotope fractionation between the total DIC pool and water as a function of the solution pH, reported as $1000\ln\alpha^{18O}_{BaCO3\text{-}H2O}$, along with estimated values for HCO_3^- (29.41 ± 0.04) and CO_3^{2-} (23.70 ± 0.29). (C) The Δ_{63} values predicted from *ab initio* calculations for pH values greater than 8. Predicted equilibrium calcite values are shown for comparison. (D) DIC β^{18O} from *ab initio* calculations for pH values greater than 8. (E) Evidence for a salinity effect on ^{13}C–^{18}O bond order of the DIC pool from theoretical calculations, and comparison to predicted calcite value. Results are shown for salinities ranging from 0–50 and for temperatures of 25 °C. (F) The same pattern is predicted for DIC β^{18O}.

0.713‰ and 0.650‰, respectively. The composition of the two species differs by 0.063 ± 0.006‰, and this difference is the same irregardless of what AFF is used. Preliminary results in a conference abstract on witherite reports a similar offset between HCO_3^- and CO_3^{2-} (~0.04‰; Guo et al., 2012).

The observed slope in our data for a regression of Δ_{47} against $\delta^{18}O$ for samples grown at variable pH is 0.011 ± 0.001 (Fig. 3**A**), reflecting changes in the equilibrium stable isotopic compositions of the DIC pool. A different slope is reported by Tang et al. (2014) for samples grown at low temperatures and at pH > 10. Due to the timescale (and temperature and pH) of their experiments, they argued the DIC pool for these samples had not attained isotopic equilibrium. Their samples grown at pH > 10 exhibit a negative Δ_{47}–$\delta^{18}O$ slope consistent with CO_2 hydrolysis (Fig. 3**C**), with a value of −0.016 to −0.07, depending on which populations of data are used to define the slope. This CO_2 hydrolysis slope is significantly steeper than the pH effect slope reported here, and opposite in sign (Fig. 3A).

Thus, we suggest that DIC speciation effects can potentially result in inaccurate temperature estimates of minerals and that comparison of the Δ_{47}–$\delta^{18}O$ slope with experimental data may be a means for identifying such effects in other datasets including in cultured and field-collected samples. We compared our results for equilibrium DIC species compositions to predictions from previous studies synthesizing calcite under controlled temperatures (blue bars in Fig. 2, Table 2) (Ghosh et al., 2006; Dennis and Schrag, 2010; Zaarur et al., 2013). Using end-member Δ_{47} values for HCO_3^- and CO_3^{2-} derived in the present study with published temperature calibrations is a means for assessing the potential systematic errors that DIC speciation can introduce into temperature calculations. For example, if temperatures are calculated using the published Δ_{47}–temperature calibration for synthetic calcite (Ghosh et al., 2006 recalculated on the absolute reference frame), we estimate apparent precipitation temperatures ranging from 22.2 to 41.3 °C, despite all samples having been grown at 25 °C. Application of other published calibrations for synthetic calcite (e.g., Dennis and Schrag, 2010; Zaarur et al.,

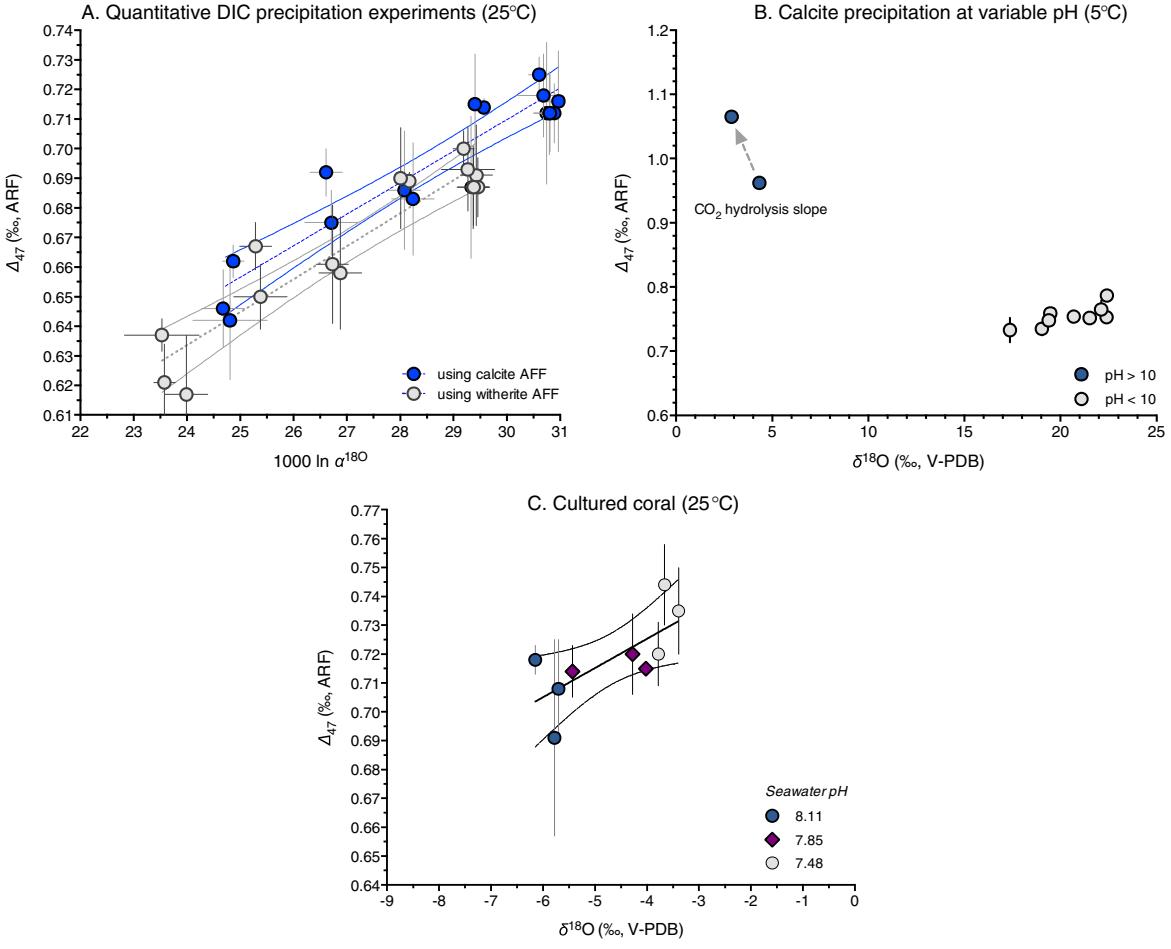

Fig. 3. Experimental data constrain slopes in Δ_{47}–$\delta^{18}O$. (A) Δ_{47}–$\delta^{18}O$ slope for witherite precipitation experiments from DIC pools equilibrated at different pH and at 25 °C (this study). Slope is 0.011 ± 0.001. (B) Data from Tang et al. (2014) for 5 °C showing CO_2 hydrolysis slope (samples grown at pH > 10). Slope is −0.011 to −0.07 (depending on what all data are used to calculate values). (C) Slope for coral (*O. arbuscula*) cultured at 25 °C and variable pH showing slope similar to dataset in panel A. Slope is 0.010 ± 0.03. Additional data for coral are also shown in Fig. 6.

2013; Tang et al., 2014) produces similar results as the calibrations intersect at a point near 25 °C (Table 2).

3.1.3. Theoretical modeling of equilibrium isotope compositions of DIC species and comparison to predictions for carbonate minerals

We used first-principles electronic structure theory to predict isotopic compositions of DIC species and carbonate minerals. Modeling solvated species is complex and can be computationally intensive. Further, the inclusion of explicit waters of hydration is critical for accurate estimation of vibrational properties and isotopic partitioning (Rudolph et al., 2006; Rustad et al., 2008; Zeebe, 2009). Therefore, we performed a study that simulated aqueous and crystalline chemical environments and compared techniques for capturing solvation effects. These methods, validation tests, and an in depth discussion of some of our initial theoretical results are presented elsewhere (Hill et al., 2014).

3.1.3.1. Theoretical results for carbonate minerals. We include in Table 3 a comparison of calcite and aragonite calculations using two different basis sets. It should be noted the aragonite and calcite values calculated using a smaller basis set are systematically offset to lower values than those calculated using a larger basis set, with a difference of −0.034‰ and −0.027‰ at 25 °C for aragonite and calcite, respectively. It is therefore likely that the witherite values from our theoretical calculations may underestimate equilibrium Δ_{63} and Δ_{47} values. For comparison, model calculations done using the same basis set yield witherite values that are about 0.01‰ lower than those of calcite, while Schauble et al. (2006) found calcite and witherite were indistinguishable (a nominal difference of about 0.001‰). Nonetheless, we note that given the uncertainties in model calculations and experimental datasets, the theoretical predictions are within error of the observations.

3.1.3.2. Theoretical results for DIC species and comparison to carbonate minerals and to experimental results. According to the preferred model (optimizing computational time vs. accuracy), at 25 °C there is a Δ_{63} difference of 0.033‰ between HCO_3^- and CO_3^{2-}. This difference varies with temperature, ranging from 0.037‰ at 0 °C to 0.030‰ at 50 °C. The composition of calcite falls between HCO_3^- and CO_3^{2-} (Fig. 4). The simulated oxygen isotopic compositions of these species also bracket calcite values. For example, the predicted $1000\ln\alpha^{18O}_{CO3-H20}$ is 22.6, and $1000\ln\alpha^{18O}_{HCO3-H20}$ is 29.3. The predicted $1000\ln\alpha^{18O}$ difference of 6.7 between CO_3^{2-} and HCO_3^- is similar to our experimental results (5.7 ± 0.3).

The same trends simulated in Δ_{63} are expected in the Δ_{47} of CO_2 extracted from aqueous species and calcite. All model results indicate equilibrium fractionations between DIC species should be measurable given analytical uncertainties. Furthermore, the equilibrium temperature dependence of Δ_{63} for each DIC species and carbonate mineral is similar in slope, although each species has a distinct intercept (Fig. 4; Table 3).

Two discrepancies exist between the model and experimental results. Our experimental results for these two

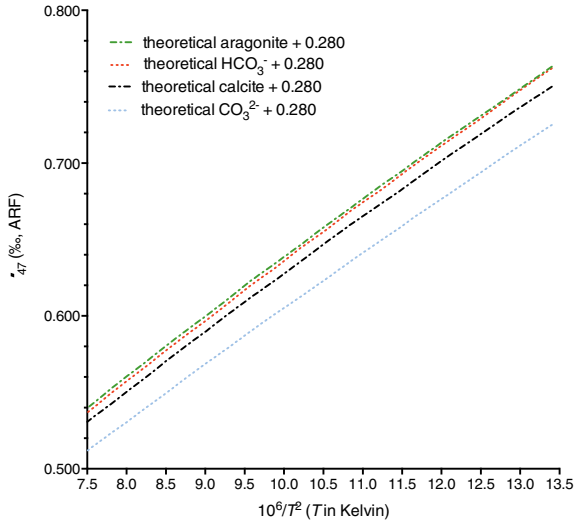

Fig. 4. Comparison of theoretical predictions from this study of Δ_{47} of DIC species and carbonate minerals based on modeled Δ_{63} and acid digestion fractionation factor for calcite of 0.280‰. At a given temperature, aragonite and HCO_3^- have higher values than calcite, and CO_3^{2-} has the lowest value. CO_3^{2-} slope = 0.0364 ± 0.0001, int. = 0.2403 ± 0.0013; HCO_3^- slope = 0.0384 ± 0.0002, int. = 0.2504 ± 0.0017; calcite slope = 0.0375 ± 0.0002, int. = 0.2508 ± 0.0019; aragonite slope = 0.0381 ± 0.0002, int. = 0.2558 ± 0.0020.

aqueous species indicate a compositional difference in Δ_{47} (and presumably Δ_{63}) of 0.063 ± 0.006‰, which is larger than theoretical predictions but in the same direction. The observed slope in a regression of Δ_{47} against $\delta^{18}O$ for samples grown at variable pH (Fig. 3A) of 0.011 ± 0.001 is slightly greater than theoretical predictions (0.004–0.007). However, the trends in the model results match what is observed in our experiments.

3.2. Calculations exploring potential for DIC speciation effects on the isotopic composition of DIC pool

The experiments and models presented above indicate CO_3^{2-} and HCO_3^- differ from one another in both Δ_{63} and $\delta^{18}O$ when equilibrated at the same temperature (and in the case of $\delta^{18}O$, the same water). If at equilibrium, both Δ_{63} and $\delta^{18}O$ in the DIC pool depend primarily on DIC speciation at a given temperature, reflecting differences in isotopic effects on vibrational energies of CO_3^{2-} and HCO_3^-. Thus, our results provide a framework for understanding the relationship between pH and the isotopic signatures of the DIC pool for solutions that attain thermodynamic equilibrium.

Fig. 5 shows the combined effects of both pH and temperature on stable isotope signatures of the composite DIC pool. In these calculations, both the proportions of DIC species and their isotopic compositions reflect thermodynamic homogeneous equilibrium (in water of fixed $\delta^{18}O$). In contrast, predictions for equilibrium Δ_{63} mineral compositions are affected only by temperature and are independent of pH. Similarly, mineral $\delta^{18}O$ values in heterogeneous equilibrium with water of fixed $\delta^{18}O$ are affected by temperature and not pH.

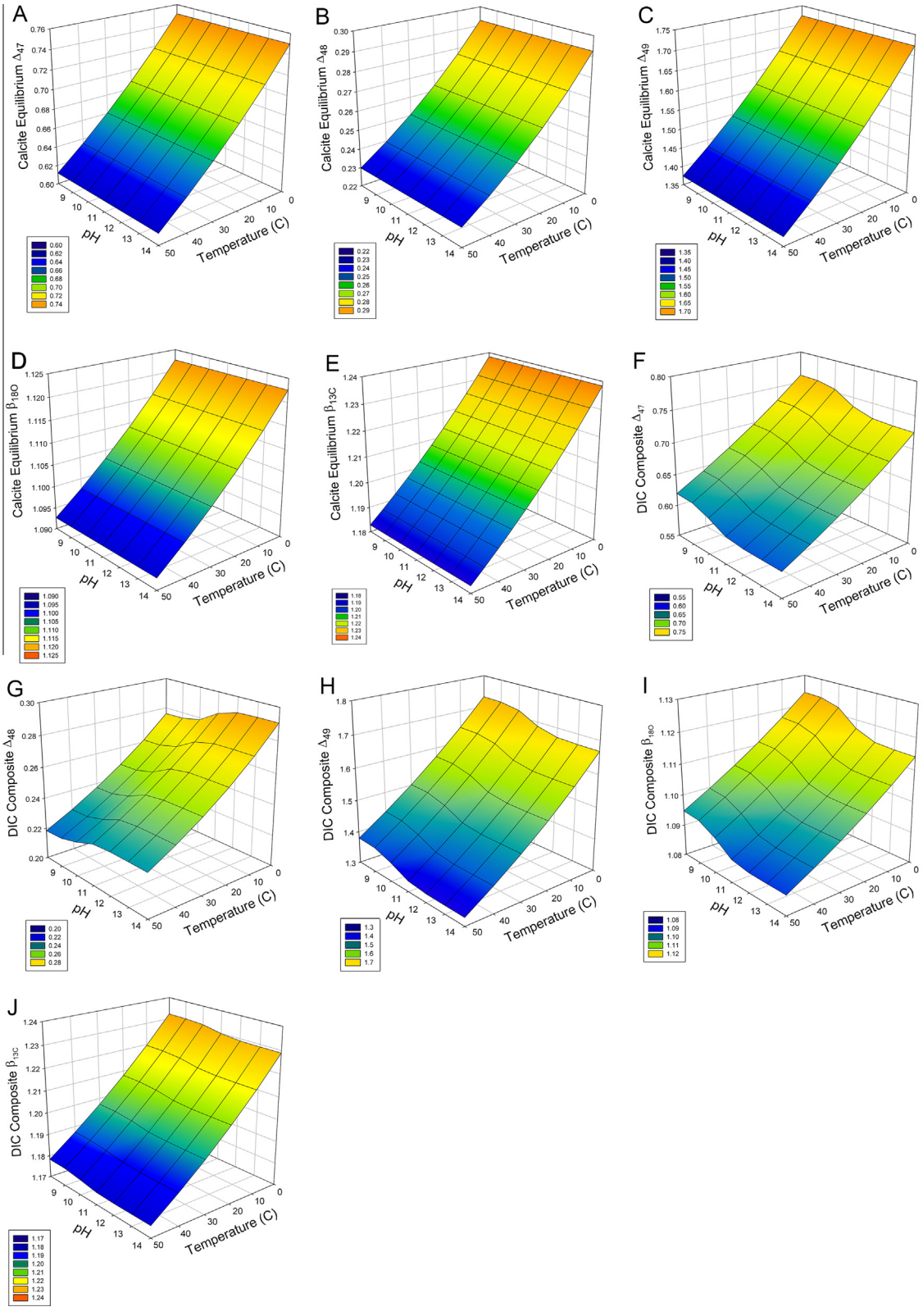

Although the primary control on DIC speciation is pH, the pK values for the dissociation constants K_1 and K_2 have been empirically demonstrated to vary as a function of salinity, temperature, and pressure, as do K_i values for other acid–base systems (Dickson and Millero, 1987; Millero et al., 2006). An increase in either salinity

Fig. 5. Theoretical calculations from this study showing equilibrium stable isotopic composition of calcite and DIC pool as a function of temperature and pH. *Ab initio* calculations demonstrate that both temperature and DIC speciation affect the abundance of multiply substituted isotopologues as well as oxygen isotope fractionations in solution. Results are shown for temperatures from 0 to 50 °C. Calcite AFF are used for the conversion of Δ_{63}, Δ_{64}, and Δ_{65} to Δ_{47}, Δ_{48}, and Δ_{49} values. (A) Combined effects of temperature and pH on the Δ_{47} of the calcite mineral lattice. In this case, we consider homogenous equilibrium in the solid phase exclusively, and therefore effects of solution chemistry are not considered. (B–D) Similar renderings for Δ_{48}, Δ_{49}, and β^{18O} respectively, for calcite. (E–H) *Ab initio* calculations of equilibrium Δ_{47}, Δ_{48}, Δ_{49}, and β^{18O} values for the DIC pool for pH values greater than 7. Note the stepped structure of the multiply substituted isotopologue distribution in DIC as a function of temperature and pH. This structure is not seen in calcite as the mineral lattice is modeled as having attained complete isotopic equilibrium. All figures represent calculations for a salinity of 0. Note that changing salinity could have potentially amplifying or dampen the magnitude of the isotope effects shown here due to salinity-dependence of DIC speciation as seen in Fig. 1.

(Fig. 1A) or temperature (Fig. 1B) decreases K_1 and K_2, the constants of the equations governing the relative abundances of DIC species. These increases lower the pH values when HCO_3^- and CO_3^{2-} ions are most abundant. An increase in salinity also slightly lowers the maximum abundance of HCO_3^- ions. Salinity has a somewhat greater influence than temperature on DIC speciation (over the range of natural variation in surface waters observed on earth) (Millero et al., 2006). The effects of salinity can be explained by the non-ideal behavior of DIC species and other dissolved constituents: changing salinity influences interactions between different ions (e.g., ion pairs), impacting the activity of carbonate species.

As the salinity effect on DIC speciation is well-established (Dickson and Millero, 1987; Millero et al., 2006), given the difference in the isotopic compositions of DIC species, one would expect a salinity effect on the clumped-isotope and oxygen-isotope compositions of the total DIC pool. We calculated the effect of changing salinity on the composition of a DIC pool at equilibrium. These calculations utilize a general relationship between pK_i values and salinity (Millero et al., 2006). The influence of specific ions, and the role of common ion pairs in seawater and brines, on clumped isotope signatures of the DIC pool is an area for future research.

Because increased salinity lowers the pH where HCO_3^- and CO_3^{2-} are equal in concentration, and increases the abundance of CO_3^{2-} at a given pH, it also lowers the pH at which the Δ_{63} value of the DIC pool is equal to equilibrium calcite. This pH value (the pH at which the equilibrium Δ_{63} of calcite equals the equilibrium Δ_{63} of the DIC pool) is defined as the "crossover pH" (Hill et al., 2014). The effect of salinity on the isotopic composition of the DIC pool can be significant. For example, at 25 °C the predicted crossover pH for fresh water ($S = 0$) is ~10, compared to 8.7 for seawater ($S = 35$) (where the grey line cross the curved lines in Fig. 2E–F). If the effects of salinity on DIC speciation affect a growing mineral and not considered, then mineral precipitation temperature might be underestimated or overestimated.

In addition to salinity, the pK values are also sensitive to temperature. We predict temperature influences the composition of the DIC pool through two mechanisms: primarily because Δ_{63} values of each DIC species are thermodynamically controlled, and secondarily because of the effect of temperature on K_i. Thus, as temperature increases, DIC peaks shift to lower pH values, slightly decreasing the crossover pH.

In summary, the effect of increasing salinity is to shift the entire Δ_{63} curve of the composite DIC pool toward lower pH, thus lowering the clumped crossover pH. Temperature has a similar effect, with the entire Δ_{63} curve shifted to lower values due to the thermal dependence of K_i and the consequences on DIC Δ_{63}. Further examples of the effects on Δ_{47} and inferred temperatures, if not taken into account, are described in Section 4.3.1.

3.3. Observations of disequilibrium clumped isotope signatures in carbonate minerals arising from a pH effect

We observed a Δ_{47}–$\delta^{18}O$ slope in cultured temperate coral that is similar to what was observed in our quantitative DIC precipitation experiments. We measured 9 specimens of the zooxanthellate coral *O. arbuscula* that were cultured at 25 °C and at seawater pH ranging from ~7.5 to 8.2 (Ries et al., 2009, 2010). Linear extension rates ranged from ~1100 μm/year for the lowest pH treatment, to ~7800 μm/year for the other pH treatments.

The analyzed coral exhibits a range of Δ_{47} and $\delta^{18}O$ values that are not significantly correlated with changes in growth rate ($p = 0.1088$ for Δ_{47} and 0.0855 for $\delta^{18}O$) (Fig. 6A and B). Both Δ_{47} and $\delta^{18}O$ do vary inversely with seawater pH (Fig. 6C and D, Table S4). This variation is consistent with disequilibrium mineral precipitation given that ambient conditions should not have varied significantly between treatments.

Scleractinian corals were investigated for this study because they are known to exhibit disequilibrium mineral signatures or "vital effects" in $\delta^{18}O$ (McConnaughey, 1989; Rollion-Bard et al., 2003, 2011; Adkins et al., 2003) and in Δ_{47} (Ghosh et al., 2006; Saenger et al., 2012). It is debated whether these isotopic signatures originate from kinetic effects associated with CO_2 hydrolysis due to different isotopologues of CO_2 reacting at variable rates (McConnaughey, 1989; Saenger et al., 2012), or from pH effects on the stable isotope composition of the DIC pool (Adkins et al., 2003; Rollion-Bard et al., 2003, 2011). Direct microelectrode measurements of the calcifying fluids of two temperate species indicates they elevate pH of their calcifying fluid by 1 (Al-Horani et al., 2003) to 2 units (Ries, 2011) relative to seawater pH, and that changes in seawater pH can be reflected in calcifying fluid pH, which was reduced in corals grown in acidified seawater (Ries, 2011).

To distinguish between the two competing interpretations for the origin of isotopic vital effect in these corals,

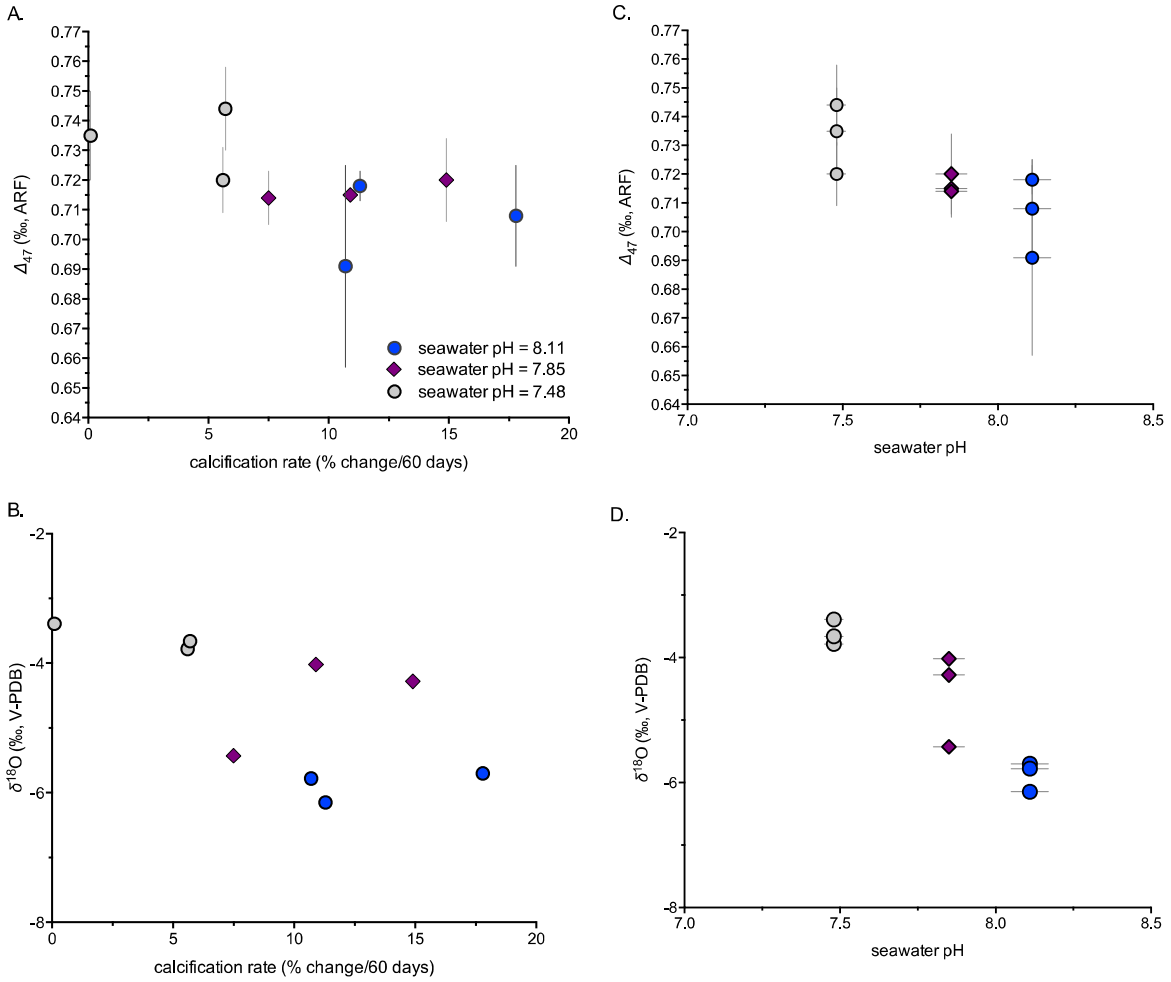

Fig. 6. The Δ_{47} and $\delta^{18}O$ composition of aragonite produced by the temperate scleractinian coral *Oculina arbuscula* varies inversely with seawater pH, but is not affected by coral calcification rate when pH is held constant. Crossplot of Δ_{47} and $\delta^{18}O$ is shown in Fig. 3C. Δ_{47} values predicted from empirical calibrations range from 0.687‰ to 0.703‰ (Table 2). (A) Δ_{47} vs. pH for the coral *O. arbuscula*. (B) $\delta^{18}O$ vs. pH for the coral *O. arbuscula*. (C) Δ_{47} vs. calcification rate for the coral *O. arbuscula*. (D) $\delta^{18}O$ vs. calcification rate for the coral *O. arbuscula*.

we first compare our experimentally determined pH effect from the witherite precipitation experiments to data from experiments that constrain the CO_2 hydrolysis slope, albeit with few data points (Tang et al., 2014). The positive $\Delta_{47}/\delta^{18}O$ slope observed in the witherite precipitation experiments (Fig. 3A; 0.011 ± 0.001) is in the opposite direction of the CO_2 hydrolysis slope (Fig. 3B), and is also smaller in absolute magnitude. Notably, the $\Delta_{47}/\delta^{18}O$ slope for the coral dataset (Fig. 3C; 0.010 ± 0.003) is in the same direction and similar in magnitude to what we observe in our witherite experiments, consistent with differences in calcifying fluid pH driving the observed range of mineral Δ_{47} and $\delta^{18}O$ values measured in this taxa. Specimens grown at the lowest seawater pH have the highest Δ_{47} and $\delta^{18}O$ values, consistent with HCO_3^- comprising a larger proportion of the DIC pool at lower pH, thereby influencing the isotopic composition of the coral skeleton. Thus our isotopic data are consistent with microelectrode results (for other species of temperate coral) that indicate elevated calcifying fluid pH.

Note the temperate coral species we studied, that were grown at variable pH and constant temperature, exhibit a different type of no-equilibrium isotope effects to those reported in different coral taxa that experienced also experienced different ambient temperatures (Saenger et al., 2012). This previous study reported data for coral taxa that exhibited a negative $\Delta_{47}/\delta^{18}O$ slope consistent with disequilibrium originating from CO_2 hydrolysis (Fig. 8A). A difference in $\Delta_{47}/\delta^{18}O$ slopes between coral taxa is likely related to variable carbon sources and calcification strategies that particular species have likely evolved to cope with the range of pH and temperatures in their ambient environments, as well as differences in growth rate.

3.4. Observations of possible equilibrium clumped isotope signatures in carbonate minerals?

3.4.1. Synthetic calcites grown at variable temperature

Synthetic calcites grown by the active degassing method over temperatures ranging from 0.5–50 °C yield a

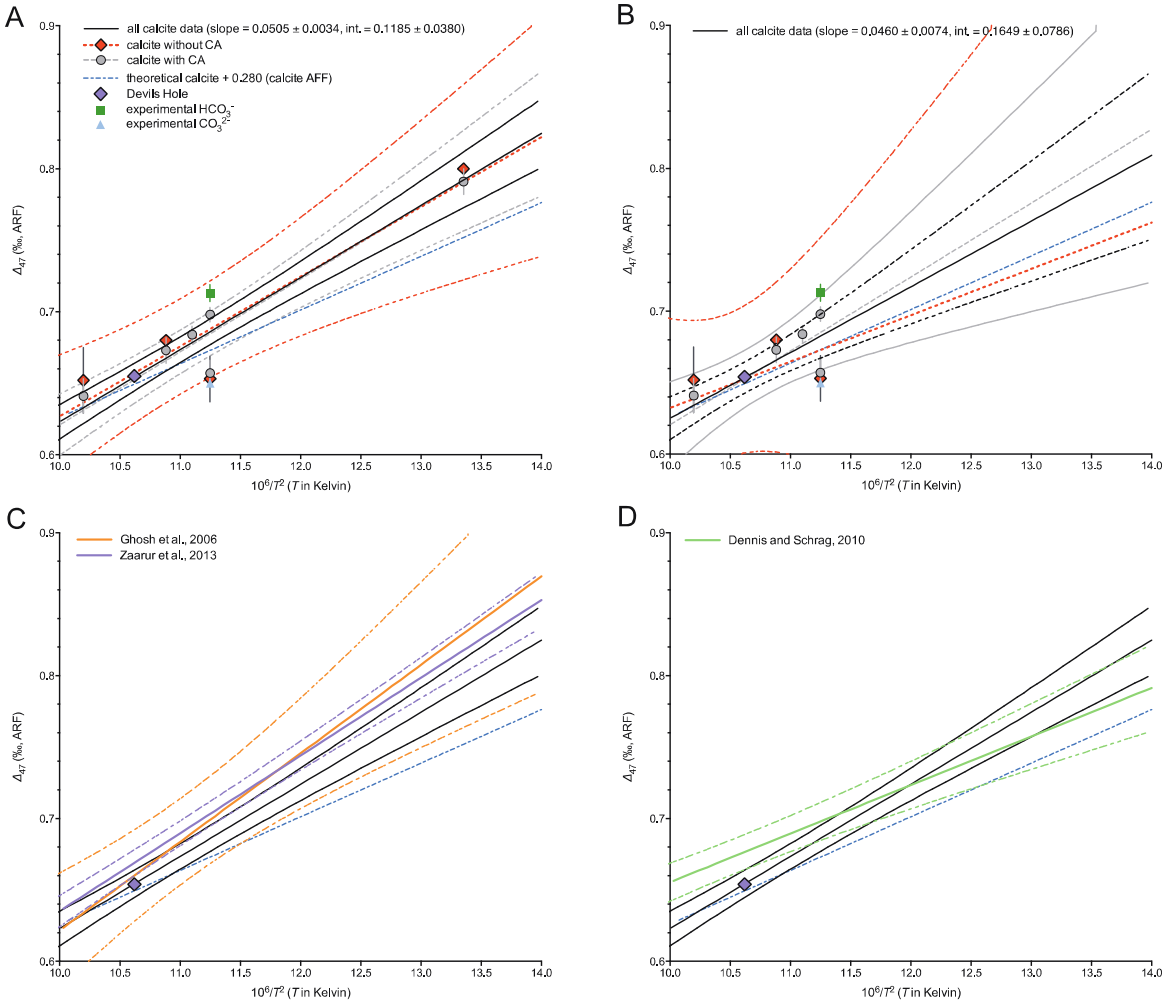

Fig. 7. Δ_{47} data for synthetic calcite compared to different datasets. (A) Data for samples grown at temperatures ranging from 0.5 to 50 °C with and without the enzyme carbonic anhydrase. Regression lines for synthetic calcite and 95% confidence intervals are shown. Slope for all calcite data = 0.0505 ± 0.0034, int. = 0.1185 ± 0.0380. Results for the two types of experiments (with and without the enzyme carbonic anhydrase) are identical, and also overlap with our theoretical predictions for equilibrium calcite and with the Devils Hole values, consistent with equilibrium calcite precipitation. Regression through combined dataset for synthetic calcite (both with and without carbonic anhydrase) also shown. (B) Same as Panel A with low temperature data points removed. Slope for all calcite data = 0.0460 ± 0.0074, int. = 0.1649 ± 0.0786. (C) Comparison of regression through all synthetic calcite data from Panel A with published experimental calibrations with a steep slope (Ghosh et al., 2006 and Zaarur et al., 2013 on ARF). (D) Comparison of regression through all synthetic calcite data from Panel A with published experimental calibration with a shallow slope (Dennis and Schrag, 2010 on ARF). (For interpretation of the references to colour in this figure legend, the reader is referred to the web version of this article.)

Δ_{47}–temperature relationship of $\Delta_{47} = (0.0488 \pm 0.0081) \times 10^6/T^2 + (0.1386 \pm 0.0906)$ (red lines in Fig. 7A). If these synthetic calcites had grown out of equilibrium, we would predict these carbonates might have distinct clumped isotope compositions from carbonates grown in the presence of carbonic anhydrase. Calcites grown in the presence of the enzyme carbonic anhydrase yield the statistically indistinguishable relationship of: $\Delta_{47} = (0.0509 \pm 0.0054) \times 10^6/T^2 + (0.1118 \pm 0.0606)$ (grey lines in Fig. 7A). The observation that these calibrations are statistically indistinguishable, and that the results overlap with our theoretical predictions for calcite at lattice equilibrium (blue line in Fig. 7A), is consistent with the precipitated crystals from these experiments attaining lattice equilibrium. The combination of both datasets yields the following calibration: $\Delta_{47} = (0.0505 \pm 0.0034) \times 10^6/T^2 + (0.1185 \pm 0.0380)$ (black line Fig. 7A; Table 4). This calibration is intermediate in composition between our experimentally-constrained values of HCO_3^- and CO_3^{2-}, consistent with our theoretical predictions. This calibration is slightly shallower in slope and has a higher intercept than what has been reported by Ghosh et al. (2006) and Zaarur et al. (2013), although these differences are relatively small and are not statistically significant (Fig. 7C, Table 4). It is also similar to the published all biogenics calibration from Eagle et al. (2013a,b). Our results are notably steeper than the inorganic calcite calibrations published by Dennis and Schrag (2010) (Fig. 7D) and Tang et al. (2014) (Table 4).

The calibration results are influenced strongly by the low-temperature data points. If the low-temperature data

Table 4
Regressions through calibration datasets. All samples digested at 90 °C use the acid digestion fractionation factor of Henkes et al. (2013). Note that other published calibration datasets exhibiting a steep slop include calibrations for foraminifera from Tripati et al. (2010) and Grauel et al. (2013), prepared via phosphoric acid digestion at 25 and 70 °C respectively. Shallow calibration slopes are observed in synthetic calcite and aragonite reported by Dennis and Schrag (2010) digested at 70 °C, Defliese et al. (2015) digested at a range of temperatures, and for biogenic carbonates reported by Wacker et al. (2014) that was digested at both 25 and 90 °C.

Characteristics	Type of material	Calibration	Slope	Intercept	Acid digestion temperature and device
Steep slope, shallow intercept	Synthetic	Inorganic calcite – this study	0.0505 ± 0.0034	0.1185 ± 0.0380	90 °C
	Synthetic	Inorganic calcite (excluding low T) – this study	0.0460 ± 0.0074	0.1649 ± 0.0786	90 °C
	Synthetic	Inorganic calcite – recalculated by Eagle et al. (2013a) using data from Ghosh et al., 2006	0.0620 ± 0.0099	0.0021 ± 0.1095	25 °C
	Synthetic	Inorganic carbonates – recalculated using data from Zaarur et al., 2013	0.0544 ± 0.0028	0.0911 ± 0.0318	25 °C
	Biogenic	All biogenic data – Eagle et al. (2013a)	0.0559 ± 0.0019	0.0708 ± 0.0232	Both 25 and 90 °C
	Biogenic	Deep-sea coral (mainly Desmophylum) – Thiagarajan et al. (2011)			25 °C
	Biogenic	Deep-sea coral (scleractinian) – Kimball et al. (2013)	n/a	n/a	90 °C
Shallow slope, high intercept	Synthetic	Inorganic calcite – Tang et al. (2014)	0.0387 ± 0.0072	0.2532 ± 0.0829	90 and 100 °C
	Biogenic	Bivalve mollusks and brachiopods – Henkes et al. (2013)	0.0327	0.3286	Mainly 90, some 25 °C
	Biogenic	Bivalve mollusks – Eagle et al. (2013a,b)	0.0362 ± 0.0044	0.3140 ± 0.0527	90 °C
	Biogenic	Deep-sea coral (gorgonian) – Kimball et al. (2013)	n/a	n/a	90 °C

are excluded, the slopes for all of the calibrations shallow and the intercepts steepen. The relationship observed for the samples grown without the enzyme present becomes $\Delta_{47} = (0.0385 \pm 0.0108) \times 10^6/T^2 + (0.2448 \pm 0.1138)$ (Fig. 7B), more similar to the published shallow slope, high intercept calibrations for synthetic calcite (Dennis and Schrag, 2010; Tang et al., 2014) (Table 4). The experiments with the enzyme yield a calibration of $\Delta_{47} = (0.0517 \pm 0.0115) \times 10^6/T^2 + (0.1033 \pm 0.1236)$ (Fig. 7B). The combination of both datasets yields a calibration of $\Delta_{47} = (0.0460 \pm 0.0034) \times 10^6/T^2 + (0.1649 \pm 0.0786)$ (Table 4). These latter two calibration relationships are more similar to the published high slope, low intercept calibration for synthetic calcite (Ghosh et al., 2006; Zaarur et al., 2013), the all biogenics calibration from Eagle et al. (2013a) produced mainly at 25 °C with some 90 °C data, and other biogenic calibrations based on acid digestion at both 25 and 90 °C (Table 4). The origin of these differences in calibration slope and intercept (Table 4) are not yet well understood (e.g., Dennis et al., 2011), but may be explained in part by the different protocols used for sample digestion and gas purification (Defliese et al., 2015), and/or by kinetic effects. Our calibration data, however, do not support the hypothesis that all data produced using the 90 °C acid digestion reaction produces the shallow slope of Dennis and Schrag, 2010 and Tang et al. (2014).

3.4.2. In search of mineral equilibrium in nature: Devils Hole

The Devils Hole calcite vein, a natural precipitate from groundwater, may represent an ideal natural sample of a mineral that has attained lattice equilibrium (i.e., the isotopic composition is dependent only on temperature and is independent of solution chemistry), or closely approaches it (Coplen, 2007; Gabitov et al., 2012; Watkins et al., 2013). Coplen (2007) used Devils Hole data to conclude that most synthetic and biogenic carbonates used in other calibration studies grew too rapidly to attain equilibrium mineral $\delta^{18}O$ signatures. Therefore, the Devils Hole calcite vein provides an important reference point for clumped-isotope measurements, and an interesting test case to compare with our theoretical and experimental results (Fig. 7, Tables 2, S7).

We present data from Devils Hole core that has previously been studied (Winograd et al., 1988; Coplen, 2007), and note that clumped isotope data for samples from the Devils Hole system that were produced using a 25 °C offline acid digestion reaction has recently been published (Kluge et al., 2014). Due to an ongoing debate on the role of sample reaction methodology (Defliese et al., 2015) and mass spectrometry corrections (He et al., 2012), we regard our newly-generated data as an important reference point for measurements carried out using 90 °C acid digestion reactions and the automated online gas purification system (Passey et al., 2010) rather than the 25 °C offline acid digestion reaction (Ghosh et al., 2006; Zaarur et al., 2013; Kluge et al., 2014).

We made 27 measurements of six samples of the Devils Hole calcite vein from core DH-2. These samples were collected by the U.S. Geological Survey at Ash Meadows, Nevada (Winograd et al., 1988). Waters at the site have been monitored for temperature, pH, and other chemical parameters (Plummer et al., 2000). It is assumed that calcite precipitated from waters with a pH and temperature similar to present-day values of 7.4 (HCO_3^--dominated) and 33.7 ± 0.2 °C (Coplen, 2007).

Uranium-series ages for DH-2 were used to estimate growth rates for the vein of 0.1–0.8 μm/year (Winograd et al., 2006). These rates are at least 1–4 orders of magnitude slower than average values calculated for a range of calcitic and aragonitic organisms, including deep-sea coral, tropical coral, foraminifera, mollusks, and sponges (Gussone et al., 2005; Roark et al., 2006; Coplen, 2007; Houlbrèque et al., 2010; Hill et al., 2011; Saenger et al., 2012). It has been hypothesized that slow growth rates yield carbonate minerals that are in equilibrium with co-existing waters. In the case of $\delta^{18}O$, calcium isotopes, and Sr/Ca ratios, slow crystal growth facilitates mineral–fluid equilibrium (Tarutani et al., 1969; Kim and O'Neil, 1997; Watson, 2004; DePaolo, 2011; Gabitov et al., 2012).

Both glacial and interglacial samples were analyzed for this study, with measured $\delta^{18}O$ and $\delta^{13}C$ ratios in agreement with previous work (Winograd et al., 1997 as reported by Landwehr et al., 1997). We determined mineral Δ_{47} values ranging from 0.643 ± 0.011‰ to 0.670 ± 0.007‰. Notably, vein Δ_{47} values are statistically distinct from HCO_3^- (Fig. 7, Table 2). Mean glacial values are 0.644 ± 0.002‰ (adjusted to 25 °C), and the non-AFF corrected value is 0.552‰. Mean interglacial values are 0.644 ± 0.005‰, and the non-AFF corrected value is 0.567‰. The glacial and interglacial values are not statistically distinguishable from each other (Table S5) and therefore are shown averaged together in Fig. 7 and Table 2, with a mean value of 0.655 ± 0.004‰, and a non-AFF corrected value of 0.563‰, which we take to reflect calcite lattice equilibrium for growth at 33.7 °C. The vein values overlap with our theoretical predictions for calcite and the synthetic calcite calibration from this study, and with the published synthetic carbonate calibrations from Zaarur et al. (2013) and Ghosh et al. (2006), all of which yield estimates of growth temperatures for the vein within error of modern groundwater temperatures.

Using the combined calibration reported above (slope of 0.0505 and intercept of 0.1185) that was generated in this study, which is similar to the synthetic calcite calibrations of Ghosh et al., 2006 and Zaarur et al., 2013 (Table 4), we estimate a mean growth temperature of 33.7 ± 1.2 °C with values ranging from 29.5 to 37.1 °C (Table S5). Kluge et al. (2014) reports clumped isotope data for the same system, and also found no significant differences between glacial and interglacial samples. Their reconstructed temperatures, using the calibration of Zaarur et al. (2013), indicate an average growth temperature of 30.6 ± 1.6 °C with values ranging from 28.6 to 33.6 °C. The fact that reconstructed growth temperatures from both studies are within error of the modern cave temperature is consistent with equilibrium precipitation.

4. DISCUSSION

We discuss some previous models of mechanisms of equilibrium and disequilibrium signatures in carbonate

minerals, propose a model that may be capable of explaining the observed isotopic data, and discuss implications for our understanding of disequilibrium clumped isotope signatures in minerals. Finally we discuss the outlook for clumped isotope thermometry and describe additional processes that should be investigated in future studies.

4.1. Evaluation of mechanisms of equilibrium and disequilibrium signatures in carbonate minerals

4.1.1. Quantitative precipitation of DIC pool

Zeebe (1999, 2007) discusses how if the DIC pool has been quantitatively precipitated, the $\delta^{18}O$ of foraminiferal calcite will inherit the weighted average composition of the DIC pool from which they calcify. Furthermore, the weighted average $\delta^{18}O$ value for the total DIC pool will only equal the equilibrium calcite value at a single solution pH; all other pH values will yield a disequilibrium calcite value. Zeebe's model can be readily adapted to predict the Δ_{63} of calcite in cases where the mineral also records the pH-dependent isotopic composition of the DIC pool (Tripati et al., 2010).

4.1.2. Growth entrapment model

The growth entrapment model describes how the composition of growing crystals is influenced by processes near the solution/solid interface that can produce non-equilibrium mineral values. This model (Watson and Liang, 1995; Watson, 2004; Gabitov et al., 2012) posits the near-surface region of a crystal can have a distinct composition from the bulk crystal lattice. The near-surface region of the solid may grow in equilibrium with co-existing fluid, but produce a composition that differs from equilibrium crystal lattice values. Thus, an "equilibrium" crystal can only be produced if growth is sufficiently slow that transport of atoms between the near-surface and core lattice through solid-state diffusion can establish an equilibrium composition in the newly-formed solid before it is effectively isolated by further growth. In rapidly-growing crystals, the burial of the near-surface region may result in disequilibrium mineral compositions.

The possible mechanisms by which solid-state diffusion might occur are debated. The process may be linked to the occurrence of vacancy defects, which are influenced by reactions occurring at crystal growth surfaces (Labotka et al., 2004, 2011; Watson, 2004; Passey and Henkes, 2012). The diffusivity of the bulk mineral may be higher in the near-surface region where lattice vacancies are concentrated due to interactions between unsatisfied charges and water molecules at the interface of the solution boundary layer and the crystal surface (Kronenberg et al., 1984; Teng et al., 2000; Watson and Baxter, 2007; Labotka et al., 2011).

However, it is still a problem that rates of solid-state diffusion are expected to be extremely low at Earth surface temperatures, so low that quantitative experiments are very difficult. We are unaware of empirically determined oxygen and carbon diffusivities at such temperatures. Further, we are unaware of data describing the distribution of ^{13}C and ^{18}O isotopes that would enable comparison of near-surface and bulk lattice bond ordering in crystals grown at different rates. Even so, grain boundary and lattice diffusivities of oxygen and carbon in calcite have been measured at high temperatures (Farver, 1994; Farver and Yund, 1998) and derived Arrhenius laws can be extrapolated to low temperatures (e.g., Watson, 2004). Based on this extrapolation (Watson, 2004; Gabitov et al., 2012), it has been argued that near-surface lattice diffusion may occur within calcite at low temperatures (e.g., 25 °C), with site-to-site jumps of atoms within a near-surface layer. Specifically, this mechanism has been invoked (Watson, 2004; Gabitov and Watson, 2006; Gabitov et al., 2008, 2012) to explain $\delta^{18}O$, calcium isotope, and trace element data in carbonate minerals from several studies (Stipp et al., 1992; Fenter et al., 2000; Gabitov and Watson, 2006; Gaetani and Cohen, 2006; Gabitov et al., 2008, 2012; Tang et al., 2008a,b).

4.1.3. Surface reaction kinetics

Another model for non-equilibrium mineral composition is based on surface reaction-controlled kinetics. This model emphasizes molecular exchange fluxes at the mineral–solution interface and does not explicitly consider the effects of solid-state diffusion (DePaolo, 2011). The model considers surface reactivity as a competition between molecular exchange fluxes: the mineral–solution exchange rate versus the net precipitation rate. These two dimensions can be used to describe the kinetic and equilibrium partitioning of singly-substituted isotopes occurring between two phases (e.g., mineral and fluid). DePaolo (2011) focuses on first-order reaction kinetics articulated through a forward and reverse step, each of which has an associated kinetic isotope effect. The net precipitation rate is the difference between these steps. Equilibrium is achieved as net growth approaches zero, and disequilibrium occurs when growth rates are high.

4.1.4. Ion-by-ion growth model

The surface kinetic model has been adapted to consider how the ion-by-ion growth of crystals is influenced by several processes: solution pH, surface speciation at the hydrated mineral surface, as well as the attachment and detachment of ions to and from reactive features (i.e., kink sites along step edges) (Nielsen et al., 2012; Watkins et al., 2013). The model is constrained by atomic force microscopy data describing step velocities in calcite, and forward and backward rates of attachment for different ions (Wolthers et al., 2012). The model assumes attachment and detachment rate coefficients for HCO_3^- and CO_3^{2-} isotopologues. It has been used to explain some of the same geochemical data described by the growth entrapment model.

4.1.5. Comparison of existing models with data

It is unclear if any of the models can explain the combination of Δ_{47} and $\delta^{18}O$ signatures in natural materials. Although both the quantitative DIC precipitation and surface kinetic models predict circumstances in which a crystal attains Δ_{63} and $\delta^{18}O$ equilibrium, or Δ_{63} and $\delta^{18}O$ disequilibrium, the models have yet to explain observations of Δ_{63}

lattice equilibrium and large amounts of $\delta^{18}O$ disequilibrium in carbonate minerals, as reported for deep-sea corals and foraminifera (Ghosh et al., 2006; Tripati et al., 2010; Thiagarajan et al., 2011; Affek and Zaarur, 2014). The ion-by-ion growth model does predict kinetic effects on mineral $\delta^{18}O$ as a function of precipitation rate (Watkins et al., 2013). However, if adapted to also predict mineral Δ_{63} (Hunt, Watkins, DePaolo, Ryerson, and Tripati, unpublished results), it would predict detectable but relatively minor kinetic clumped-isotope effects and moderate $\delta^{18}O$ disequilibrium in minerals growing rapidly from a DIC pool at thermodynamic equilibrium, similar to what is observed in many carbonates (Tripati et al., 2010) but in contrast to what is observed in deep-sea coral (Ghosh et al., 2006; Thiagarajan et al., 2011). Although the growth entrapment model does provide a mechanism that could explain observations of both deep-sea coral and foraminifera, it lacks support from physical evidence for solid-state diffusion of oxygen and carbon isotopes over relevant timescales at Earth surface temperatures (Fairchild and Baker, 2012).

4.1.6. An interfacial model

We propose a conceptual model that may be capable of explaining observed Δ_{47} and $\delta^{18}O$ data. It considers an additional dimension to the ion-by-ion growth model: bond reordering at the crystal–solution interface. This model therefore also draws on elements of the growth entrapment model and assumes, as others have shown, the interface to be simultaneously part of the crystal surface and part of the solution (Fenter and Sturchio, 2004, 2012; Geissbühler et al., 2004; Fenter et al., 2013). Any atom/molecule/moiety at the interface will therefore be sensitive to changes in the structure of the mineral surface and the aqueous solution.

Three factors are important in this model: solution composition, chemical reactions in the interfacial region (e.g., surface equilibria, attachment and detachment rates of different isotopologues to the crystal surface) including processes resulting in bond reordering, and growth rate. In solution, HCO_3^- and/or CO_3^{2-} at the interface may be at equilibrium for a given temperature. HCO_3^- may be converted to CO_3^{2-}, but the newly-formed CO_3^{2-} (referred to as $(H)CO_3^{2-}$) may be incorporated into a rapidly-growing crystal before the ion has time to reach a temperature-dependent equilibrium for CO_3^{2-}. The model also postulates $(H)CO_3^-$ and/or CO_3^{2-} may themselves retain isotopic compositions reflecting the slow kinetics of other processes (e.g., the hydration and/or hydroxylation of CO_2).

The interfacial model focuses on surface equilibria as a critical principle governing isotope signatures in minerals, as they dictate the degree of ion attachment/detachment to carbonate mineral surfaces. The extent of ionic coverage on the crystal surface depends on solution concentration, surface equilibrium constants, and surface charge. The specific pathways and rates of reaction for different isotopologues of DIC species (e.g., attachment/detachment rates to carbonate mineral surfaces) remain unknown and are an important target for future studies. For instance, it is possible that bond reordering could occur in the interfacial environment while an anion is adsorbed but waiting for a Ca kink site to desolvate. Alternatively, there may be a reordering of clumped-isotope signatures in CO_3^{2-} groups attached in the outer monolayer of the crystal, approaching temperature-dependent mineral equilibrium values. X-ray experiments have shown distortions in the orientation of carbonate in the interfacial region (Geissbühler et al., 2004), and those distortions might promote isotopic exchange.

4.1.7. Predictions of the interfacial model

Although the specific reaction pathways are presently unknown, the Δ_{47} data presented here may provide some evidence to support a highly dynamic interfacial environment for carbonate minerals. If ^{13}C–^{18}O bond reordering occurs at the solution–mineral interface, we predict Δ_{63} lattice equilibrium may be attained, when crystal growth rates are sufficiently slow so as to not bury the interfacial region. In this slow-growth scenario, reactions occurring at the interface may have sufficient time to allow an initial disequilibrium mineral signature to evolve towards crystal lattice equilibrium. For example, precipitation rates equivalent to the Devils Hole vein (0.1–0.8 μm/year) for calcite growing at ~25–35 °C would be sufficiently slow to attain lattice equilibrium. Under such circumstances, where mineral precipitation occurs sufficiently slowly, solution chemistry is therefore unlikely to be an important factor in isotope partitioning.

Another specific prediction of the model is that, due to bond reordering in the interfacial region, minerals growing at slow rates may attain Δ_{63} lattice equilibrium while retaining $\delta^{18}O$ disequilibrium within the crystal. The observations of Δ_{63} lattice equilibrium and large amounts of $\delta^{18}O$ disequilibrium in aragonitic deep-sea corals may indicate that internal scrambling can occur within the interfacial region. This prediction is further supported by work on hematite that yielded some analogous results, and indicated that the extent of oxygen mixing on surfaces is much greater than has been realized (Henderson et al., 1998).

A future test could be performed to determine if interfacial reordering processes are relevant for attainment of mineral equilibrium values during growth at Earth-surface temperatures. Specifically, is mineral-specific Δ_{47} equilibrium observed in very slowly growing, or moderately slowly-grown (i.e., intermediate between Devil's Hole and scleractinian coral), natural samples containing $\delta^{18}O$ mineral disequilibrium? Another test could include synthetic mineral precipitation experiments where mineralogy is controlled and temperature, pH, and growth rate are varied.

4.2. Interpreting datasets to identify if there are disequilibrium clumped isotope signatures in minerals

The interfacial model implies that under conditions of "slow" growth, such as those approximated by Devils Hole vein, crystal lattices are likely to attain equilibrium. We define "rapid" or "fast" precipitation as rates at which isotopic equilibrium within a crystal is not reached, such as those of the corals that were analyzed. The actual value of growth rate that might demarcate the boundary between "slow" and "rapid" precipitation will vary depending on the conditions of mineral growth (e.g., physical and

chemical conditions of the solution including pH and temperature, surface equilibria, growth rates that influence burial of the interfacial region, and processes influencing the development of kink sites and mineral defects).

Our experimental results indicate a difference in bond order between HCO_3^- and CO_3^{2-} ions of ~0.05–0.07‰ (2 s.e.), a compositional difference that could influence rapidly-grown carbonate minerals. We suggest disequilibrium mineral compositions may arise due to rapid mineral growth, either from a DIC pool at equilibrium or at disequilibrium (i.e., HCO_3^- and CO_3^{2-} sourced from CO_2 hydrolysis) as has previously been asserted (Tripati et al., 2010; Saenger et al., 2012; Tang et al., 2014). These results further emphasize the need to consider the effects of growth environment, solution chemistry, surface equilibria, reordering in the interfacial region, and crystal growth rate when interpreting Δ_{47} and $\delta^{18}O$ values of carbonates. Unfortunately, most published clumped-isotope datasets (including inorganic calibration studies) lack information on growth environment, such as solution pH, calcification pH, and/or crystal growth rate. Such ancillary data will be critical for future studies to precisely constrain which environmental factors are reflected in the clumped and oxygen isotopic signatures of carbonate minerals.

The present model provides a framework for interpreting published datasets, and offers some testable hypotheses as described in Section 4.1.7. We note that many field-collected samples (Eagle et al., 2010; Passey et al., 2010; Tripati et al., 2010; Thiagarajan et al., 2011) have Δ_{47} values consistent with predictions from calibrations for synthetic carbonate minerals. Thus it is possible that many, but not all (Affek et al., 2008; Daëron et al., 2011; Saenger et al., 2012), carbonates that have been surveyed to date have grown slowly enough to have reached nominal mineral equilibrium values. Alternatively, most field-collected and synthetic carbonates may have grown rapidly and recorded mineral disequilibrium clumped-isotope signatures from a DIC pool at equilibrium and at an intermediate HCO_3^--dominated pH, so that at a given temperature, the Δ_{63} value (and $\delta^{18}O$) for the DIC pool is similar to that of equilibrium calcite. Indeed, most biogenic and abiogenic carbonates are generally considered to have grown rapidly, except for certain cases such as the Devils Hole vein (Winograd et al., 1992, 2006; Coplen, 2007; Dietzel et al., 2009).

4.3. Outlook for clumped-isotope thermometry

The results of this study suggest that solution chemistry and growth rates are of broad importance to the interpretation of stable isotope values in carbonate minerals. At a given temperature, if minerals grow at slow enough rates to have attained the "lattice equilibrium" limit, then their Δ_{47} will be independent of growth rate and solution chemistry, even if they exhibit disequilibrium in $\delta^{18}O$. If minerals grow rapidly enough to have attained a "kinetic" limit, then their Δ_{47} will also be independent of growth rate and will reflect solution chemistry and/or surface speciation reactions (e.g., solution pH). Over an intermediate range of growth rates, Δ_{47} will be affected by solution chemistry, surface speciation reactions, growth rate, and interfacial reactions.

Given the potential for solution chemistry effects, to ensure high-accuracy, high-precision temperature reconstructions from Δ_{47} or $\delta^{18}O$, it is critical to have studies of modern systematics for different types of carbonates, a careful selection of samples, and/or some constraints on the environment of formation. Rather than assuming mineral lattice equilibrium has been attained in many calibration datasets, including for biogenic carbonates, it is possible that the associated studies may have recorded temperature-dependent clumping and the $\delta^{18}O$ composition of HCO_3^--dominated DIC pools. If so, this does not preclude the utility of Δ_{47} and $\delta^{18}O$ values in carbonates for geothermometry; instead, it means that material-specific calibrations are important. Additionally when considering natural samples from past environments, it would be useful to consider the potential magnitude of changes in Δ_{47} and $\delta^{18}O$ that solution chemistry may have imparted.

4.3.1. Potential scope of solution chemistry effects

For potential applications of Δ_{47} thermometry to processes in the shallow crust, the effects of solution chemistry may be large in some extreme scenarios, but are likely small in environments with relatively constant conditions such as seawater. For example, in applications to ancient samples from most surface and subsurface environments where we do not know what temperature, solution chemistry, or growth rate was, the maximum combined effect of pH, salinity, and temperature on Δ_{47} is on the order of 0.08–0.11‰ in an extreme case (e.g., cold freshwater at high latitudes with $S = 0$, $T = 0$ °C, pH = ~7.5 vs. warm hypersaline brine environments with $S \geqslant 50$, $T = 25$ °C, and pH = ~10) which could equate to an error in temperatures of 20 °C or more. If considering a more representative range of conditions associated with terrestrial and marine surface waters ($S = 0$, pH = ~7.0 vs. $S = 35$, pH = ~8.2), at a given temperature, there may be ~0.01–0.02‰ effects on the Δ_{47} of the DIC pool, with seawater having higher values than freshwater, although individual cationic effects may also be important. These effects are going to be modulated by growth rate. Thus under extremes of growth rate, solution chemistry effects may not be detectable which may explain observations such as those recently reported by Kluge and John (2015).

In geological samples from ancient environments with relatively small fluctuations in pH and salinity, the consequent effects of solution chemistry on DIC speciation and measured mineral Δ_{47} values are unlikely to be discernable. Depending on mineral growth rates, the effects of pH and salinity may not be measurable for most marine inorganic and biogenic carbonate minerals precipitating from a range of open ocean conditions. We have performed calculations to illustrate the potential effects on Δ_{47} datasets from the tropical oceans at different time periods (Table 5) that show the effects of pH and salinity on Δ_{47} values should be small to negligible. If tropical carbonates from the Last Glacial Maximum formed from a DIC pool similar to seawater in composition (and not elevated to higher pH as has been observed in foraminifera - de Nooijer et al., 2009), then

Table 5
Estimates of maximum possible influence of changing pH and salinity on Δ_{47} values of DIC pool that could be inherited by rapidly-growing tropical marine carbonates. Values are based on our experimental and model-based estimates of bond order in bicarbonate and carbonate ions from this study. Calculated Δ_{63} values for the DIC pool use HCO_3^- values that are 0.035 to 0.083‰ heavier than CO_3^{2-}, K_1 and K_2 values (Millero et al., 2006), and assume pH values ranging from 8.3 to 8.5 (Last Glacial Maximum) or 7.4 to 8.5 (other time periods), salinity values ranging from 30 to 35, and temperatures ranging from 25 to 30.

Time interval	Possible effect (‰)
pH effects for Cenozoic or earlier	0.0021–0.0210
pH effects for Last Glacial Maximum	0.0021–0.0075
Salinity effects for Cenozoic	0.0001–0.0019
Salinity effects for Last Glacial Maximum	0.0003–0.0015
Combined pH and salinity – Cenozoic	0.0070–0.0212
Combined pH and salinity – Last Glacial Maximum	0.0025–0.0084

tropical sea surface temperature estimates from Δ_{47} thermometry might be subtly biased towards overestimating temperatures due to the occurrence of higher pH and higher salinity waters; combined pH and salinity effects might influence Δ_{47} values by a maximum of ~0.002–0.008‰ (equivalent to a few tenths of a degree to ~1.2 °C). During earlier time periods, changing tropical surface seawater pH would influence the Δ_{47} of DIC by 0.002–0.021‰ (Pearson and Palmer, 2000; Pearson et al., 2009; Roberts and Tripati, 2009; Tripati et al., 2009, 2011), while changing surface water salinity from 30 to 35 could result in as much as a 0.002‰ effect. The combined effects of both parameters in earlier time periods would range from 0.004‰ to 0.021‰. Thus, minerals that grew rapidly in either of these time periods might have recorded seawater DIC speciation effects, resulting in small but systematic biases in temperature reconstructions.

We note that although it is important to consider the pH and salinity of environmental waters, we do not expect the $\delta^{18}O$ or Δ_{47} composition of biologically-formed minerals to be passive tracers recording ambient seawater. The potential for biological modification of pH at the site of mineral growth needs to be considered. At least some calcifiers (certain species of corals and foraminifera) are known to maintain calcifying fluid pH values significantly different from seawater and may retain the ability to buffer their internal pH from changes in the environment over fairly large ranges (Al-Horani et al., 2003; de Nooijer et al., 2009; Ries, 2011). This could minimize artifacts introduced from changes in ambient pH in foraminiferal records.

4.3.2. The utility of measuring multiple stable isotope signatures for geothermometry

These results suggest that in both marine and terrestrial settings, calibration data from modern calcifying organisms (or from inorganic phases of a particular type) can empirically constrain whether crystal growth is sufficiently rapid compared to the timescale for lattice equilibration, and thus whether solution chemistry is likely to be important. "Rapid" growth was observed in samples of temperate coral measured in this study. "Slow" growth was inferred for the Devils Hole vein.

Furthermore, combining multiple stable isotope signatures can help identify the source of mineral disequilibrium. For example, in a plot of mineral Δ_{47} vs. $\delta^{18}O$, CO_2 hydrolysis and solution pH effects are predicted to lie in different quadrants (Figs. 3, 8A). The influence of pH can be discerned with the same approach used to interrogate the coral data in the present study. Therefore, paired analysis of Δ_{47} and $\delta^{18}O$ data within modern calcifying taxa should help identify what types of fossil carbonates (e.g., which taxa) are most appropriate for paleotemperature reconstructions.

Other rare multiply-substituted isotopologues in carbonate minerals would also be useful for temperature reconstructions. Our calculations show other clumped species should also be sensitive to temperature and DIC speciation, as well as to other kinetic processes fractionating isotopes such as CO_2 hydration and hydroxylation (Fig. 5). Fig. 8 illustrates that it may be possible to identify and quantify disequilibrium components in field-collected carbonate minerals using coupled measurements of Δ_{47}, Δ_{48}, and Δ_{49}. The approach is analogous to pairing Δ_{47} with $\delta^{18}O$.

We propose that in carbonates known to have formed in marine or freshwater settings, it should be feasible to estimate simultaneously temperature and the $\delta^{18}O$ of water, as well as have an independent check on the attainment of mineral equilibrium. Although it is not yet possible to measure *m*/*z*-48 and *m*/*z*-49 isotopologues with a high degree of precision on most gas-source mass spectrometers, a new generation of high-resolution instruments is being developed that should permit evaluation of this approach.

4.4. Additional processes that should be investigated

An area for future work is the inclusion of multiply-substituted isotopologues into models for isotopic fractionation. When taken in conjunction with our estimates of DIC species end-member compositions from this study, quantitative modeling will make predictions for the magnitude of isotope effects and the pH and growth rate dependence of Δ_{63} in minerals that can be compared to data for natural samples.

In addition to the processes we have discussed, other factors may influence crystal growth in natural systems and laboratory experiments and should be investigated. For instance, a range of ion sorption and incorporation processes could potentially affect ^{13}C–^{18}O signatures of carbonate groups in the surface monolayer of a crystal. However, to date, investigating these processes present a wide range of challenges. Studying the reactivity and structure of carbonate mineral surfaces is complex, as it must examine processes such as diffusion into hydrated surface layers,

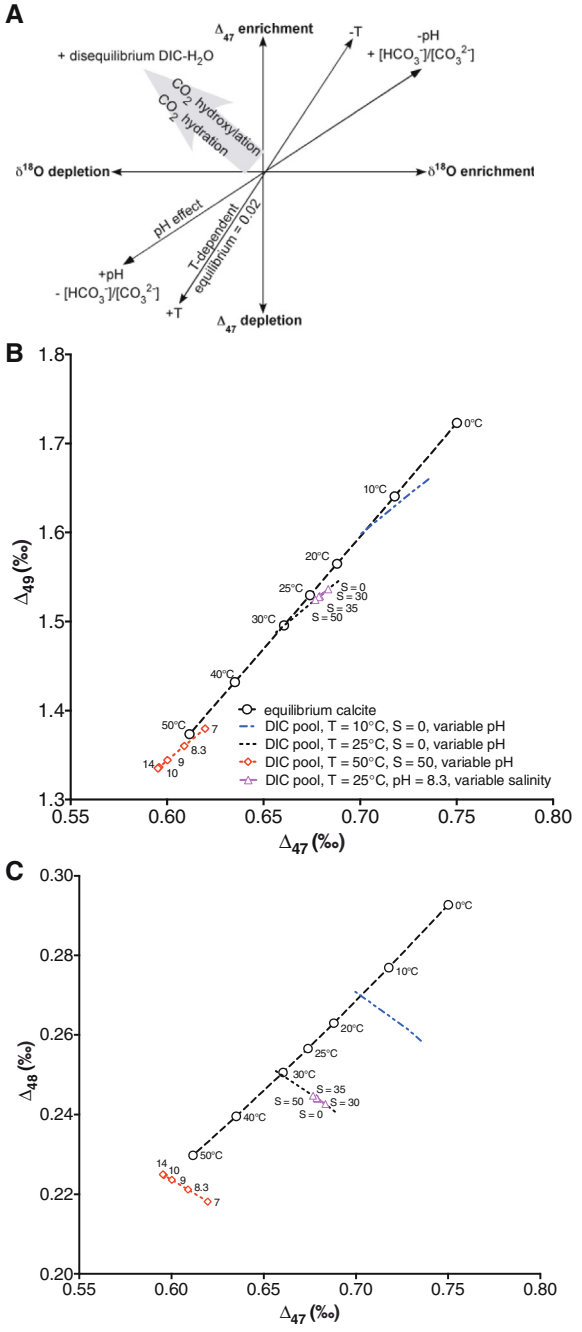

Fig. 8. Paired measurements of Δ_{47}, Δ_{48}, Δ_{49} and $\delta^{18}O$ may provide additional constraints on what processes may be driving disequilibrium in field-collected samples. (A) $\delta^{18}O$–Δ_{47} vector schematic for multiple processes. *T*-dependent equilibrium is constrained from calibrations for synthetic calcite (e.g., this study; Ghosh et al., 2006; Zaarur et al., 2013), while the slope of the pH effect is derived from Fig. 2C. (B) The Δ_{49} values of the DIC pool and non-equilibrium minerals should also exhibit process-specific correlations with Δ_{47} dependent on pH, salinity, and temperature from theory. Slope of temperature-dependent calcite mineral equilibrium is shown for comparison. (C) Same as Panel B but showing comparison of Δ_{48} and Δ_{47}.

dehydration, adsorption, desorption, bond relaxation or rupturing, and molecular rotation in the surface monolayer (Stipp et al., 1992, 1998; Van Cappellen et al., 1993; Fenter et al., 2000, 2013; Kulik, 2002; Villegas-Jiménez et al., 2009a,b; Wolthers et al., 2008, 2012). Furthermore, the surface reactions that can influence the attachment and incorporation of ions including Ca^{2+}, CO_3^{2-}, HCO_3^-, H^+, and OH^- are not well understood. The rates of attachment and detachment of different isotopologues are poorly constrained or unknown, yet are essential for developing accurate models of clumped-isotope fractionation during crystal growth. The presence of metal ions in solution that could become constituents of the lattice are also potentially important as they can change the protonation of the surface of the crystal by competing with protons and each other for reactive surface sites.

Additionally, the potential impact of ion pairs and complexing of CO_3^{2-} and HCO_3^- with common cations is unclear, as is the role of elevated hydroxyl concentrations at alkaline pH, where OH^- ions may also complex with important cations. The presence of OH^- ions at high pH enhances dehydration of Ca^{2+} and promotes surface adsorption and lattice incorporation of the cation. Further, the adsorption of OH^- at high pH can change calcite growth morphology, as inferred from atomic force microscopy and surface complexation modeling (Ruiz-Agudo et al., 2011). Other variables for controlling mineral chemistry have been identified in experiments, including growth in the presence of ligands or other organic molecules (Lebron and Suarez, 1996; Wang et al., 2009; Hamm et al., 2010; Hu et al., 2013), grain size (Kile and Eberl, 2003), and subdomains.

Amorphous precursors (Addadi et al., 2003; Politi et al., 2008; Pouget et al., 2009; Weiner et al., 2009) also play an important role in the biomineralization pathways of many organisms. The short-range ordering, dehydration, and crystallization (Radha et al., 2010; Rodriguez-Blanco et al., 2011; Bots et al., 2012) of these amorphous phases may affect isotope partitioning. Similarly, a critical step in the formation of both biogenic and abiogenic carbonate minerals involves the presence of stable prenucleation ion clusters of $CaCO_3$, existing in equilibrium with free ions and solvent. Cluster formation may be pH-dependent (Gebauer et al., 2008), and the free ion–cluster equilibrium is influenced by dissolution–reprecipitation reactions (Myerson and Trout, 2013; Wallace et al., 2013). Although these phases have been identified over the last decade as being important for understanding carbonate mineral nucleation and growth, no theoretical or experimental studies have investigated the Δ_{63} and $\delta^{18}O$ composition of amorphous calcium carbonate or prenucleation ion clusters. Assessing the importance of the above phases and processes in controlling disequilibrium stable isotopic signatures in minerals should be a target for future studies.

5. CONCLUSIONS

We show that factors aside from temperature can influence carbonate mineral Δ_{47} and $\delta^{18}O$. Based on measurements and *ab initio* calculations, we conclude that DIC speciation influences the stable isotopic composition of the DIC pool, implying that bond equilibration can occur

in solution. The composite equilibrium Δ_{63} of DIC depends primarily upon temperature and pH, and secondarily on salinity. We find a significant difference between the Δ_{63} (and $\delta^{18}O$) of aqueous HCO_3^- and CO_3^{2-}, which may impact the accuracy of reconstructed temperatures under certain conditions.

In conditions of rapid growth, solution chemistry can influence mineral Δ_{47} signatures. For example, the Δ_{47} and $\delta^{18}O$ values measured in cultured temperate scleractinian coral from this work exhibit a range of values despite being grown at a constant temperature, and vary inversely with solution pH. The slope of the $\Delta_{47}/\delta^{18}O$ relationship is consistent with a pH effect. These results imply some scatter in Δ_{47}–temperature calibrations could result from rapid growth of crystals.

Slow crystal growth favors attainment of independent Δ_{63} equilibrium in the mineral lattice. As a result, the mineral clumped-isotope signature should be independent of solution chemistry. These results are supported by our observations that slowly-grown natural calcites from the Devils Hole vein exhibit Δ_{47} values that approaches mineral equilibrium values. The isotopic composition is intermediate between HCO_3^- and CO_3^{2-}, with error bounds overlapping with our synthetic calcite calibration. We report a new Δ_{47}–temperature calibration for temperatures ranging from 0.5 to 50 °C, based upon measurements of synthetic calcites. This calibration overlaps with the Devils Hole vein, with theoretical predictions from this study for calcite at lattice equilibrium, and importantly also with previously published calibrations (Ghosh et al., 2006; Zaarur et al., 2013).

These findings help explain the origin of equilibrium and disequilibrium Δ_{47} signatures in minerals, and allow for more accurate use of clumped-isotope thermometry in geological systems. We suggest processes operating at the crystal–solution interface are likely to be important in governing whether equilibrium or disequilibrium clumped isotope signatures are attained. Growth environment, solution chemistry, surface equilibria, and precipitation rate may all play a role in dictating clumped-isotope and $\delta^{18}O$ signatures in minerals.

AUTHOR CONTRIBUTION STATEMENT

AKT designed and funded the project, made most of the measurements, provided input on modeling to postdoctoral researcher (PSH), interpreted the data and contributed to interpretations of theoretical results, guided the acid digestion study, drafted most of the figures, and wrote the paper. PSH did the theoretical calculations and contributed to interpretations of theoretical results and drafted a figure. RAE measured samples and drafted some figures. JLM conducted the heating experiments and provided a description of the methodology. JT and DH conducted the acid digestion study. EAS provided input on modeling to PH and contributed to interpretations of theoretical results. JU provided samples and fluid pH, DIC, and values of water as well as a brief description of the methodology. TBC assisted with collection and provided samples from Devils Hole. JBR provided coral samples cultured under various pH conditions, seawater chemistry data, and rates of coral calcification. AKT, JME, and REZ manage laboratories where the research was conducted. All authors contributed to discussions of results and provided edits to the manuscript.

ACKNOWLEDGEMENTS

AKT thanks the reviewers and editor for their comments, as well as Kate Ledger, Hagit Affek, Tobias Kluge, James Watkins, Jim Rustad, William Casey, Oleg Pokrovsky, Ian Fairchild, Bruce Watson, Henry Teng, Philippe Van Cappellen, Adrian Villegas-Jimenez, Andreas Luttge, Bernhardt Trout, Michael Reddy, Dan Breecker, Andrew Dickson, Gideon Henderson, Frank Millero, Justine Kimball, and Chris Roberts for discussions relevant to this work. AKT and PSH thank Ben Elliott, Anastassia Alexandrova, and Ben Schwartz for input, and Fernando R. Clemente of Gaussian, Inc., for helpful suggestions with Gaussian09. AKT acknowledges support from the Department of Energy through BES grant DE-FG02-13ER16402, a UCLA Career Development Award, a Hellman Fellowship, NSF grants EAR-0949191, EAR-1325054, ARC-1215551, and ACS grant #51182-DNI2. RAE and JBR acknowledge support from NSF grant OCE-1437166. REZ was supported by NSF grant OCE09-27089. JBR acknowledges support from NSF grant OCE-1357665 and NOAA grant NA13OAR4310186. The support of the U.S. Geological Survey National Research Program made this article possible. Any use of trade, firm, or product names is for descriptive purposes only and does not imply endorsement by the U.S. Government.

APPENDIX A. SUPPLEMENTARY DATA

Supplementary data associated with this article can be found, in the online version, at http://dx.doi.org/10.1016/j.gca.2015.06.021.

REFERENCES

Addadi L., Raz S. and Weiner S. (2003) Taking advantage of disorder: amorphous calcium carbonate and its roles in biomineralization. *Adv. Mater.* **15**, 959–970.

Adkins J., Boyle E., Curry W. and Lutringer A. (2003) Stable isotopes in deep-sea corals and a new mechanism for "vital effects". *Geochim. Cosmochim. Acta* **67**, 1129–1143.

Affek H. (2013) Clumped isotopic equilibrium and the rate of isotope exchange between CO_2 and water. *Am. J. Sci.* **313**, 309–325.

Affek H. and Zaarur S. (2014) Kinetic isotope effect in CO2 degassing: Insight from clumped and oxygen isotopes in laboratory precipitation experiments. *Geochim. Cosmochim. Acta* **143**, 319–330.

Affek H., Bar-Matthews M., Ayalon A., Matthews A. and Eiler J. (2008) Glacial/interglacial temperature variations in Soreq cave speleothems as recorded by "clumped isotope" thermometry. *Geochim. Cosmochim. Acta* **72**, 5351–5360.

Affek H., Matthews A., Ayalon A., Bar-Matthews M., Burstyn Y., Zaarur S. and Zilberman T. (2014) Accounting for kinetic isotope effects in Soreq Cave (Israel) speleothems. *Geochim. Cosmochim. Acta* **143**, 303–318.

Al-Horani F., Al-Moghrabi S. and de Beer D. (2003) Microsensor study of photosynthesis and calcification in the scleractinian coral, Galaxea fascicularis: active internal carbon cycle. *J. Exp. Mar. Biol. Ecol.* **288**, 1–15.

Beck W., Grossman E. and Morse J. (2005) Experimental studies of oxygen isotope fractionation in the carbonic acid system at 15°, 25° and 40°C. *Geochim. Cosmochim. Acta* **69**, 3493–3503.

Bots P., Benning L., Rodriguez-Blanco J.-D., Roncal-Herrero T. and Shaw S. (2012) Mechanistic Insights into the crystallization of amorphous calcium carbonate (ACC). *Cryst. Growth Des.* **12**, 3806–3814.

Böttcher M. (1996) $^{18}O/^{16}O$ and $^{13}C/^{12}C$ fractionation during the reaction of carbonates with phosphoric acid: effects of cationic substitution and reaction temperature. *Isot. Environ. Health Stud.* **32**, 299–305.

Came R. E., Eiler J. M., Veizer J., Azmy K., Brand U. and Weidman C. R. (2007) Coupling of surface temperatures and atmospheric CO_2 concentrations during the Palaeozoic era. *Nature* **449**(7159), 198–201.

Chandra S. (1981) Interaction of $BaCl_2$ and $BaCO_3$ at elevated temperatures. *J. Am. Ceram. Soc.* **64**, C-101–C-102.

Coplen T. (2007) Calibration of the calcite–water oxygen-isotope geothermometer at Devils Hole, Nevada, a natural laboratory. *Geochim. Cosmochim. Acta* **71**, 3948–3957.

Coplen T. (2011) Guidelines and recommended terms for expression of stable-isotope-ratio and gas-ratio measurement results. *Rapid Commun. Mass Spectrom.* **25**, 2538–2560.

Csank A., Tripati A., Patterson W., Eagle R., Rybczynski N., Ballantyne A. and Eiler J. (2011) Estimates of Arctic land surface temperatures during the early Pliocene from two novel proxies. *Earth Planet. Sci. Lett.* **304**, 291–299.

Daëron M., Guo W., Eiler J., Genty D., Blamart D., Boch R., Drysdale R., Maire R., Wainer K. and Zanchetta G. (2011) $^{13}C^{18}O$ clumping in speleothems: observations from natural caves and precipitation experiments. *Geochim. Cosmochim. Acta* **75**, 3303–3317.

Defliese W., Hren M. and Lohmann K. (2015) Compositional and temperature effects of phosphoric acid fractionation on Δ_{47} analysis and implications for discrepant calibrations. *Chem. Geol.* **296**, 51–60.

Dennis K. and Schrag D. (2010) Clumped isotope thermometry of carbonatites as an indicator of diagenetic alteration. *Geochim. Cosmochim. Acta* **74**, 4110–4122.

Dennis K., Affek H., Passey B., Schrag D. and Eiler J. (2011) Defining an absolute reference frame for "clumped" isotope studies of CO_2. *Geochim. Cosmochim. Acta* **75**, 7117–7131.

DePaolo D. (2011) Surface kinetic model for isotopic and trace element fractionation during precipitation of calcite from aqueous solutions. *Geochim. Cosmochim. Acta* **75**, 1039–1056.

Dickson A. and Millero F. (1987) A comparison of the equilibrium constants for the dissociation of carbonic acid in seawater media. *Deep-Sea Res.* **34**, 1733–1743.

Dietzel M., Tang J., Leis A. and Köhler S. (2009) Oxygen isotopic fractionation during inorganic calcite precipitation – effects of temperature, precipitation rate and pH. *Chem. Geol.* **268**, 107–115.

Eagle R., Schauble E., Tripati A., Tütken T., Hulbert R. and Eiler J. (2010) Body temperatures of modern and extinct vertebrates from ^{13}C–^{18}O bond abundances in bioapatite. *Proc. Natl. Acad. Sci.* **107**, 10377–10382.

Eagle R., Tutken T., Martin T., Tripati A., Fricke H., Connely M., Cifelli R. and Eiler J. (2011) Dinosaur body temperatures determined from isotopic (^{13}C–^{18}O) ordering in fossil biominerals. *Science* **333**, 443–445.

Eagle R., Eiler J., Tripati A., Ries J., Freitas P., Hiebenthal C., Wanamaker, Jr, A., Taviani M., Elliot M. and Marenssi S. (2013a) The influence of temperature and seawater carbonate saturation state on ^{13}C–^{18}O bond ordering in bivalve mollusks. *Biogeosciences* **10**, 4591–4606.

Eagle R., Risi C., Mitchell J., Neelin D., Eiler J., Seibt U., Li G. and Tripati A. (2013b) High regional climate sensitivity over continental China inferred from glacial-recent changes in temperature and the hydrologic cycle. *Proc. Natl. Acad. Sci.* **110**, 8813–8818.

Eiler J. (2011) Paleoclimate reconstruction using carbonate clumped isotope thermometry. *Quatern. Sci. Rev.* **30**, 3575–3588.

Fairchild I. and Baker A. (2012) Geochemistry of speleothems. In *Speleothem Science*. John Wiley & Sons, Ltd, pp. 245–289.

Farver J. (1994) Oxygen self-diffusion in calcite: dependence on temperature and water fugacity. *Earth Planet. Sci. Lett.* **121**, 575–587.

Farver J. and Yund R. (1998) Oxygen grain boundary diffusion in natural and hot-pressed calcite aggregates. *Earth Planet. Sci. Lett.* **161**, 189–200.

Fenter P., Geissbühler P., DiMasi E., Srajer G., Sorensen L. and Sturchio N. (2000) Surface speciation of calcite observed in situ by high-resolution X-ray reflectivity. *Geochim. Cosmochim. Acta* **64**, 1221–1228.

Fenter P., Kerisit S., Raiteri P. and Gale J. (2013) Is the calcite–water interface understood? Direct comparisons of molecular dynamics simulations with specular X-ray reflectivity data. *J. Phys. Chem. C* **117**, 5028–5042.

Fenter P. and Sturchio N. (2004) Mineral–water interfacial structures revealed by synchrotron X-ray scattering. *Prog. Surf. Sci.* **77**, 171–258.

Fenter P. and Sturchio N. (2012) Calcite (1 0 4)–water interface structure, revisited. *Geochim. Cosmochim. Acta* **97**, 58–69.

Gabitov R. and Watson E. B. (2006) Partitioning of strontium between calcite and fluid. *Geochem. Geophys. Geosyst.* **7**. http://dx.doi.org/10.1029/2005GC001216.

Gabitov R., Gaetani G., Watson E. B., Cohen A. and Ehrlich H. (2008) Experimental determination of growth rate effect on U^{6+} and Mg^{2+} partitioning between aragonite and fluid at elevated U^{6+} concentration. *Geochim. Cosmochim. Acta* **72**, 4058–4068.

Gabitov R., Watson E. B. and Sadekov A. (2012) Oxygen isotope fractionation between calcite and fluid as a function of growth rate and temperature: an in situ study. *Chem. Geol.* **306–307**, 92–102.

Gaetani G. and Cohen A. (2006) Element partitioning during precipitation of aragonite from seawater: A framework for understanding paleoproxies. *Geochim. Cosmochim. Acta* **70**, 4617–4634.

Gebauer D., Völkel A. and Cölfen H. (2008) Stable prenucleation calcium carbonate clusters. *Science* **322**, 1819–1822.

Geissbühler P., Fenter P., DiMasi E., Srajer G., Sorensen L. and Sturchio N. (2004) Three-dimensional structure of the calcite–water interface by surface X-ray scattering. *Surf. Sci.* **573**, 191–203.

Ghosh P., Adkins J., Affek H., Balta B., Guo W., Schauble E., Schrag D. and Eiler J. (2006) ^{13}C–^{18}O bonds in carbonate minerals: a new kind of paleothermometer. *Geochim. Cosmochim. Acta* **70**, 1439–1456.

Grauel A. L., Schmid T. W., Hu B., Bergami C., Capotondi L., Zhou L. and Bernasconi S. M. (2013) Calibration and application of the 'clumped isotope' thermometer to foraminifera for high-resolution climate reconstructions. *Geochim. Cosmochim. Acta* **108**, 125–140.

Guo W., Mosenfelder J., Goddard, III, W. and Eiler J. (2009) Isotopic fractionations associated with phosphoric acid digestion of carbonate minerals: insights from first-principles theoretical modeling and clumped isotope measurements. *Geochim. Cosmochim. Acta* **73**, 7203–7225.

Guo, W., Kim, S.-T., Yuan, J., Farquhar, J., Passey, B. (2012) ^{13}C–^{18}O bonds in dissolved inorganic carbon: toward a better understanding of clumped isotope thermometer in biogenic carbonates. In 22nd Annual V.M. Goldschmidt Conference, Montreal, Canada.

Gussone N., Böhm F., Eisenhauer A., Dietzel M., Heuser A., Teichert B. M. A., Reitner J., Wörheide G. and Dullo W.-C. (2005) Calcium isotope fractionation in calcite and aragonite. *Geochim. Cosmochim. Acta* **69**, 4485–4494.

Hamm L., Wallace A. and Dove P. (2010) Molecular dynamics of ion hydration in the presence of small carboxylated molecules and implications for calcification. *J. Phys. Chem. B* **114**, 10488–10495.

He B., Olack G. A. and Colman A. S. (2012) Pressure baseline correction and high-precision CO_2 clumped-isotope (Δ_{47}) measurements in bellows and micro-volume modes. *Rapid Commun. Mass Spectrom.* **26**(24), 2837–2853.

Henderson M., Joyce S. and Rustad J. (1998) Interaction of water with the (1 × 1) and (2 × 1) surfaces of α-Fe_2O_3(0 1 2). *Surf. Sci.* **417**, 66–81.

Henkes G. A., Passey B. H., Wanamaker A. D., Grossman E. L., Ambrose W. G. and Carroll M. L. (2013) Carbonate clumped isotope compositions of modern marine mollusk and brachiopod shells. *Geochim. Cosmochim. Acta* **106**, 307–325.

Hill T., Spero H., Guilderson T., LaVigne M., Clague D., Macalello S. and Jang N. (2011) Temperature and vital effect controls on bamboo coral (isididae) isotope geochemistry. *Geochem. Geophys. Geosyst.* **12**. http://dx.doi.org/10.1029/2010GC003443, Q04008, April 26, 2011.

Hill P., Tripati A. and Schauble E. (2014) Theoretical constraints on the effects of pH, salinity, and temperature on clumped isotope signatures of dissolved inorganic carbon species and carbonate minerals. *Geochim. Cosmochim. Acta*. http://dx.doi.org/10.1016/j.gca.2013.06.018, 125, 610-652.

Houlbrèque F., McCulloch M., Roark B., Guilderson T., Meibom A., Kimball J., Mortimer G., Cuif J.-P. and Dunbar R. (2010) Uranium-series dating and growth characteristics of the deep-sea scleractinian coral: Enallopsammia rostrata from the Equatorial Pacific. *Geochim. Cosmochim. Acta* **74**, 2380–2395.

Hu Q., Nielsen M., Freeman C., Hamm L., Tao J., Lee J., Han T., Becker U., Harding J., Dove P. and Yoreo J. (2013) The thermodynamics of calcite nucleation at organic interfaces: classical vs. non-classical pathways. *Faraday Discuss.* **159**, 509–523.

Huntington K., Eiler J., Affek H., Guo W., Bonifacie M., Yeung L., Thiagarajan N., Passey B., Tripati A. and Daëron M. (2009) Methods and limitations of "clumped" CO_2 isotope (Δ_{47}) analysis by gas-source isotope ratio mass spectrometry. *J. Mass Spectrom.* **44**, 1318–1329.

Kile D. and Eberl D. (2003) On the origin of size-dependent and size-independent crystal growth: Influence of advection and diffusion. *Am. Mineral.* **88**, 1514–1521.

Kim S.-T. and O'Neil J. (1997) Equilibrium and non-equilibrium oxygen isotope effects in synthetic carbonates. *Geochim. Cosmochim. Acta* **61**, 3461–3475.

Kim S.-T., Mucci A. and Taylor B. (2007) Phosphoric acid fractionation factors for calcite and aragonite between 25 and 75 °C: revisited. *Geochim. Cosmochim. Acta* **246**, 135–146.

Kimball J. B., Tripati A., Dunbar, R. B., and Eagle, R. (2013). ^{13}C–^{18}O bonding (Δ_{47}) in deep-sea corals: a calibration study. In AGU Fall Meeting Abstracts. Vol. 1, p. 1935.

Kluge T. and Affek H. P. (2012) Quantifying kinetic fractionation in Bunker Cave speleothems using Δ_{47}. *Quatern. Sci. Rev.* **49**, 82–94.

Kluge T. and John C. (2015) Effects of brine chemistry and polymorphism on clumped isotopes revealed by laboratory precipitation of mono-and multiphase calcium carbonates. *Geochim. Cosmochim. Acta* **160**, 155–168.

Kluge T., Affek H., Dublyansky Y. and Spotl C. (2014) Devils Hole paleotemperatures and implications for oxygen isotope equilibrium fractionation. *Earth Planet. Sci. Lett.* **400**, 251–260.

Kronenberg A., Yund R. and Giletti B. (1984) Carbon and oxygen diffusion in calcite: effects of Mn content and P H_2O. *Phys. Chem. Miner.* **11**, 101–112.

Kulik D. (2002) Gibbs energy minimization approach to modeling sorption equilibria at the mineral–water interface. Thermodynamic relations for multi-site-surface complexation. *Am. J. Sci.* **302**, 227–279.

Labotka T., Cole D., Riciputi L. and Fayek M. (2004) Diffusion of C and O in calcite from 0.1 to 200 MPa. *Am. Mineral.* **89**, 799–806.

Labotka T., Cole D., Fayek M. and Chacko T. (2011) An experimental study of the diffusion of C and O in calcite in mixed CO_2–H_2O fluid. *Am. Mineral.* **96**, 1262–1269.

Landwehr, J., Coplen, T., Ludwig, K., Winograd, I., Riggs, A. (1997) Data for Devils Hole Core DH-11. USGS Open-File Report 97-792 <http://pubs.usgs.gov/of/1997/ofr97-792>.

Lebron I. and Suarez D. (1996) Calcite nucleation and precipitation kinetics as affected by dissolved organic matter at 25 °C and pH > 7.5. *Geochim. Cosmochim. Acta* **60**, 2765–2776.

Lewis, E., Wallace, D., Allison, L. (1998) Program developed for CO_2 system calculations. Carbon Dioxide Information Analysis Center, managed by Lockheed Martin Energy Research Corporation for the US Department of Energy.

Loyd S., Corsetti F., Eiler J. and Tripati A. (2012) Determining the diagenetic conditions of concretion formation: assessing temperatures and pore-waters using clumped isotopes. *J. Sediment. Res.* **82**, 1006–1016.

Loyd S., Dickson J. A. D., Scholle P. and Tripati A. (2013) Extensive, uplift-related and non-fault-controlled spar precipitation in the Permian Capitan Formation. *Sed. Geol.* **298**, 17–27.

McCrea J. (1950) On the isotopic chemistry of carbonates and a paleotemperature scale. *J. Chem. Phys.* **18**, 849–857.

McConnaughey T. (1989) ^{13}C and ^{18}O isotopic disequilibrium in biological carbonates: I. Patterns. *Geochim. Cosmochim. Acta* **53**, 151–162.

Millero F., Graham T., Huang F., Bustos-Serrano H. and Pierrot D. (2006) Dissociation constants of carbonic acid in seawater as a function of salinity and temperature. *Mar. Chem.* **100**, 80–94.

Myerson A. and Trout B. (2013) Nucleation from solution. *Science* **341**, 855–856.

Nielsen L., DePaolo D. and De Yoreo J. (2012) Self-consistent ion-by-ion growth model for kinetic isotopic fractionation during calcite precipitation. *Geochim. Cosmochim. Acta* **86**, 166–181.

de Nooijer L., Toyofuku T. and Kitazato H. (2009) Foraminifera promote calcification by elevating their intracellular pH. *Proc. Natl. Acad. Sci.* **106**, 15374–15378.

Passey B. and Henkes G. (2012) Carbonate clumped isotope bond reordering and geospeedometry. *Earth Planet. Sci. Lett.* **351–352**, 223–236.

Passey B., Levin N., Cerling T., Brown F. and Eiler J. (2010) High-temperature environments of human evolution in East Africa based on bond ordering in paleosol carbonates. *Proc. Natl. Acad. Sci.* **107**, 11245–11249.

Pearson P. and Palmer M. (2000) Atmospheric carbon dioxide concentrations over the past 60 million years. *Nature* **406**, 695–699.

Pearson P., Foster G. and Wade B. (2009) Atmospheric carbon dioxide through the Eocene–Oligocene climate transition. *Nature* **461**, 1110–1113.

Pierrot, D., Lewis, E., Wallace, D. (2006) MS Excel program developed for CO2 system calculations. ORNL/CDIAC-105. Carbon Dioxide Information Analysis Center, Oak Ridge National Laboratory, US Department of Energy, Oak Ridge, Tennessee.

Plummer L., Busenberg E. and Riggs A. (2000) In-situ growth of calcite at Devils Hole, Nevada: comparison of field and laboratory rates to a 500,000 year record of near-equilibrium calcite growth. *Aquat. Geochem.* **6**, 257–274.

Politi Y., Metzler R., Abrecht M., Gilbert B., Wilt F., Sagi I., Addadi L., Weiner S. and Gilbert P. (2008) Transformation mechanism of amorphous calcium carbonate into calcite in the sea urchin larval spicule. *Proc. Natl. Acad. Sci.* **105**, 17362–17366.

Pouget E., Bomans P., Goos J., Frederik P., de With G. and Sommerdijk N. (2009) The initial stages of template-controlled $CaCO_3$ formation revealed by cryo-TEM. *Science* **323**, 1455–1458.

Radha A., Forbes T., Killian C., Gilbert P. and Navrotsky A. (2010) Transformation and crystallization energetics of synthetic and biogenic amorphous calcium carbonate. *Proc. Natl. Acad. Sci.* **107**, 16438–16443.

Ries J. (2011) A physicochemical framework for interpreting the biological calcification response to CO_2-induced ocean acidification. *Geochim. Cosmochim. Acta* **75**, 4053–4064.

Ries J., Cohen A. and McCorkle D. (2009) Marine calcifiers exhibit mixed responses to CO_2-induced ocean acidification. *Geology* **37**, 1131–1134.

Ries J., Cohen A. and McCorkle D. (2010) A nonlinear calcification response to CO_2-induced ocean acidification by the coral *Oculina arbuscula*. *Coral Reefs* **29**, 661–674.

Roark E., Guilderson T., Dunbar R. and Ingram B. (2006) Radiocarbon based ages and growth rates: Hawaiian deep sea corals. *Mar. Ecol. Prog. Ser.* **327**, 1–14.

Roberts C. and Tripati A. (2009) Modelled reconstructions of the oceanic carbonate system for different histories of atmospheric carbon dioxide during the last 20 million years. *Global Biogeochem. Cycles* **23**. http://dx.doi.org/10.1029/2008GB003310.

Rodriguez-Blanco J., Shaw S. and Benning L. (2011) The kinetics and mechanisms of amorphous calcium carbonate (ACC) crystallization to calcite, viavaterite. *Nanoscale* **3**, 265–271.

Rollion-Bard C., Chaussidon M. and France-Lanord C. (2003) pH control on oxygen isotopic composition of symbiotic corals. *Earth Planet. Sci. Lett.* **215**, 275–288.

Rollion-Bard C., Chaussidon M. and France-Lanord C. (2011) Biological control of internal pH in scleractinian corals: Implications on paleo-pH and paleo-temperature reconstructions. *C.R. Geosci.* **343**, 397–405.

Rudolph W., Fischer D. and Irmer G. (2006) Vibrational spectroscopic studies and density functional theory calculations of speciation in the CO_2–water system. *Appl. Spectrosc.* **60**, 130–144.

Ruiz-Agudo E., Putnis C., Rodriguez-Navarro C. and Putnis A. (2011) Effect of pH on calcite growth at constant ratio and supersaturation. *Geochim. Cosmochim. Acta* **75**, 284–296.

Rustad J., Nelmes S., Jackson V. and Dixon D. (2008) Quantum-chemical calculations of carbon-isotope fractionation in CO_2(g), aqueous carbonate species, and carbonate minerals. *J. Phys. Chem. A* **112**, 542–555.

Saenger C., Affek H., Felis T., Thiagarajan N., Lough J. and Holcomb M. (2012) Carbonate clumped isotope variability in shallow water corals: Temperature dependence and growth-related vital effects. *Geochim. Cosmochim. Acta* **99**, 224–242.

Schauble E., Ghosh P. and Eiler J. (2006) Preferential formation of ^{13}C–^{18}O bonds in carbonate minerals, estimated using first-principles lattice dynamics. *Geochim. Cosmochim. Acta* **70**, 2510–2529.

Spero H., Bijma J., Lea D. and Bemis B. (1997) Effect of seawater carbonate concentration on foraminiferal carbon and oxygen isotopes. *Nature* **390**, 497–500.

Stipp S., Hochella, Jr., M., Parks G. and Leckie J. (1992) Cd^{2+} uptake by calcite, solid-state diffusion, and the formation of solid–solution: Interface processes observed with near-surface sensitive techniques (XPS, LEED, and AES). *Geochim. Cosmochim. Acta* **56**, 1941–1954.

Stipp S., Konnerup-Madsen J., Franzreb K., Kulik A. and Mathieu H. (1998) Spontaneous movement of ions through calcite at standard temperature and pressure. *Nature* **396**, 356–359.

Swart P., Burns S. and Leder J. (1991) Fractionation of the stable isotopes of oxygen and carbon in carbon dioxide during the reaction of calcite with phosphoric acid as a function of temperature and technique. *Chem. Geol.* **86**, 89–96.

Tang J., Dietzel M., Böhm F., Köhler S. and Eisenhauer A. (2008a) Sr^{2+}/Ca^{2+} and $^{44}Ca/^{40}Ca$ fractionation during inorganic calcite formation: II. Ca isotopes. *Geochim. Cosmochim. Acta* **72**, 3733–3745.

Tang J., Köhler S. and Dietzel M. (2008b) Sr^{2+}/Ca^{2+} and $^{44}Ca/^{40}Ca$ fractionation during inorganic calcite formation: I. Sr incorporation. *Geochim. Cosmochim. Acta* **72**, 3718–3732.

Tang J., Dietzel M., Fernandez A., Tripati A. and Rosenheim B. (2014) Evaluation of kinetic effects on clumped isotope fractionation (Δ_{47}) during inorganic calcite precipitation. *Geochim. Cosmochim. Acta* **134**, 120–136.

Tarutani T., Clayton R. and Mayeda T. (1969) The effect of polymorphism and magnesium substitution on oxygen isotope fractionation between calcium carbonate and water. *Geochim. Cosmochim. Acta* **33**, 987–996.

Teng H., Dove P. and De Yoreo J. (2000) Kinetics of calcite growth: surface processes and relationships to macroscopic rate laws. *Geochim. Cosmochim. Acta* **64**, 2255–2266.

Thiagarajan N., Adkins J. and Eiler J. (2011) Carbonate clumped isotope thermometry of deep-sea corals and implications for vital effects. *Geochim. Cosmochim. Acta* **75**, 4416–4425.

Tripati A., Roberts C. and Eagle R. (2009) Coupling of CO_2 and ice sheet stability over major climate transitions of the last 20 million years. *Science* **326**, 1394–1397.

Tripati A., Eagle R., Thiagarajan N., Gagnon A., Bauch H., Halloran P. and Eiler J. (2010) ^{13}C–^{18}O isotope signatures and "clumped isotope" thermometry in foraminifera and coccoliths. *Geochim. Cosmochim. Acta* **74**, 5697–5717.

Tripati A., Roberts C., Eagle R. and Li G. (2011) A 20 million year record of planktic foraminiferal B/Ca ratios: systematics and uncertainties in pCO_2 reconstructions. *Geochim. Cosmochim. Acta*.

Tripati A., Sahany S., Pittman D., Eagle R., Neelin D., Mitchell J. and Beaufort L. (2014) Modern and glacial tropical snowlines controlled by sea surface temperature and atmospheric mixing. *Nat. Geosci.* **7**, 205–209.

Uchikawa J. and Zeebe R. (2012) The effect of carbonic anhydrase on the kinetics and equilibrium of the oxygen isotope exchange in the CO_2–H_2O system: implications for $\delta^{18}O$ vital effects in biogenic carbonates. *Geochim. Cosmochim. Acta* **95**, 15–34.

Uchikawa J. and Zeebe R. (2013) No discernible effect of Mg^{2+} ions on the equilibrium oxygen isotope fractionation in the CO_2–H_2O system. *Chem. Geol.* **343**, 1–11.

Usdowski E., Michaekus J., Botcher M. and Hoefs J. (1991) Factors for the oxygen isotope equilibrium fractionation between aqueous and gaseous CO_2, carbonic acid, bicarbonate, carbonate, and water (19 °C). *Zeitsch. Phys. Chem.* **170**, 237–249.

Van Cappellen P., Charlet L., Stumm W. and Wersin P. (1993) A surface complexation model of the carbonate mineral–aqueous solution interface. *Geochim. Cosmochim. Acta* **57**, 3505–3518.

Villegas-Jiménez A., Mucci A. and Paquette J. (2009a) Proton/calcium ion exchange behavior of calcite. *Phys. Chem. Chem. Phys.* **11**, 8895–8912.

Villegas-Jiménez A., Mucci A., Pokrovsky O. and Schott J. (2009b) Defining reactive sites on hydrated mineral surfaces: rhombohedral carbonate minerals. *Geochim. Cosmochim. Acta* **73**, 4326–4345.

Wacker U., Fiebig J., Tödter J., Schöne B. R., Bahr A., Friedrich O., Tütken T., Gischler E. and Joachimski M. M. (2014) Empirical calibration of the clumped isotope paleothermometer using calcites of various origins. *Geochim. Cosmochim. Acta* **141**, 127–144.

Wallace A., Hedges L., Fernandez-Martinez A., Raiteri P., Gale J., Waychunas G., Whitelam S., Banfield J. and Yoreo J. (2013) Microscopic evidence for liquid–liquid separation in supersaturated $CaCO_3$ solutions. *Science* **341**, 885–889.

Wang D., Wallace A., Yoreo J. and Dove P. (2009) Carboxylated molecules regulate magnesium content of amorphous calcium carbonates during calcification. *Proc. Natl. Acad. Sci.* **106**, 21511–21516.

Watkins J., Nielsen L., Ryerson F. and DePaolo D. (2013) The influence of kinetics on the oxygen isotope composition of calcium carbonate. *Earth Planet. Sci. Lett.* **375**, 349–360.

Watson E. B. (2004) A conceptual model for near-surface kinetic controls on the trace-element and stable isotope composition of abiogenic calcite crystals. *Geochim. Cosmochim. Acta* **68**, 1473–1488.

Watson E. B. and Baxter E. (2007) Diffusion in solid-Earth systems. *Earth Planet. Sci. Lett.* **253**, 307–327.

Watson E. B. and Liang Y. (1995) A simple model for sector zoning in slowly growing crystals: implications for growth rate and lattice diffusion, with emphasis on accessory minerals in crustal rocks. *Am. Mineral.* **80**, 1179–1187.

Weiner S., Mahamid J., Politi Y., Ma Y. and Addadi L. (2009) Overview of the amorphous precursor phase strategy in biomineralization. *Front. Mater. Sci. Chin.* **3**, 104–108.

Winograd I., Szabo B. J., Coplen T. B. and Riggs A. (1988) A 250,000-year climatic record from great basin vein calcite: implications for Milankovitch theory. *Science* **242**, 1275–1280.

Winograd I., Coplen T., Landwehr J., Riggs A., Ludwig K., Szabo B., Kolesar P. and Révész K. (1992) Continuous 500,000-year climate record from calcite vein in Devils Hole, Nevada. *Science* **258**, 255–260.

Winograd I., Landwehr J., Coplen T., Sharp W., Riggs A., Ludwig K. and Kolesar P. (2006) Devils Hole, Nevada, $\delta^{18}O$ record extended to the mid-Holocene. *Quatern. Res.* **66**, 202–212.

Winograd I. J., Landwehr J. M., Ludwig K. R., Coplen T. B. and Riggs A. C. (1997) Duration and structure of the past four interglaciations. *Quatern. Res.* **48**(2), 141–154.

Wolthers M., Charlet L. and Cappellen P. (2008) The surface chemistry of divalent metal carbonate minerals: a critical assessment of surface charge and potential data using the charge distribution multi-site ion complexation model. *Am. J. Sci.* **308**, 905–941.

Wolthers M., Nehrke G., Gustafsson J. and Van Cappellen P. (2012) Calcite growth kinetics: modeling the effect of solution stoichiometry. *Geochim. Cosmochim. Acta* **77**, 121–134.

Xirouchakis D., Hirschmann M. and Simpson J. (2001) The effect of titanium on the silica content and on mineral–liquid partitioning of mantle-equilibrated melts. *Geochim. Cosmochim. Acta* **65**, 2201–2217.

Zaarur S., Affek H. and Brandon M. (2013) A revised calibration of the clumped isotope thermometer. *Earth Planet. Sci. Lett.* **382**, 47–57.

Zeebe R. (1999) An explanation of the effect of seawater carbonate concentration on foraminiferal oxygen isotopes. *Geochim. Cosmochim. Acta* **63**, 2001–2007.

Zeebe R. (2007) An expression for the overall oxygen isotope fractionation between the sum of dissolved inorganic carbon and water. *Geochem. Geophys. Geosyst.*. http://dx.doi.org/10.1029/2003GC001663.

Zeebe R. (2009) Hydration in solution is critical for stable oxygen isotope fractionation between carbonate ion and water. *Geochim. Cosmochim. Acta* **73**, 5283–5291.

Zeebe R. and Wolf-Gladrow D. (2001). , p. 346. CO2 in Seawater: Equilibrium, Kinetics, Isotopes.

Associate editor: Miryam Bar-Matthews